

# Stimulus-induced transitions between spike-wave discharges and spindles with the modulation of thalamic reticular nucleus

Denggui Fan<sup>1</sup> · Qingyun Wang<sup>2</sup> · Jianzhong Su<sup>3</sup> · Hongguang Xi<sup>3</sup>

Received: 12 February 2017 / Revised: 11 August 2017 / Accepted: 4 September 2017 / Published online: 22 September 2017  
© Springer Science+Business Media, LLC 2017

**Abstract** It is believed that thalamic reticular nucleus (TRN) controls spindles and spike-wave discharges (SWD) in seizure or sleeping processes. The dynamical mechanisms of spatiotemporal evolutions between these two types of activity, however, are not well understood. In light of this, we first use a single-compartment thalamocortical neural field model to investigate the effects of TRN on occurrence of SWD and its transition. Results show that the increasing inhibition from TRN to specific relay nuclei (SRN) can lead to the transition of system from SWD to slow-wave oscillation. Specially, it is shown that stimulations applied in the cortical neuronal populations can also initiate the SWD and slow-wave oscillation from the resting states under the typical inhibitory intensity from TRN to SRN. Then,

we expand into a 3-compartment coupled thalamocortical model network in linear and circular structures, respectively, to explore the spatiotemporal evolutions of wave states in different compartments. The main results are: (i) for the open-ended model network, SWD induced by stimulus in the first compartment can be transformed into sleep-like slow UP-DOWN and spindle states as it propagates into the downstream compartments; (ii) for the close-ended model network, weak stimulations performed in the first compartment can result in the consistent experimentally observed spindle oscillations in all three compartments; in contrast, stronger periodic single-pulse stimulations applied in the first compartment can induce periodic transitions between SWD and spindle oscillations. Detailed investigations reveal that multi-attractor coexistence mechanism composed of SWD, spindles and background state underlies these state evolutions. What's more, in order to demonstrate the state evolution stability with respect to the topological structures of neural network, we further expand the 3-compartment coupled network into 10-compartment coupled one, with linear and circular structures, and nearest-neighbor (NN) coupled network as well as its realization of small-world (SW) topology via random rewiring, respectively. Interestingly, for the cases of linear and circular connectivities, qualitatively similar results were obtained in addition to the more irregularity of firings. However, SWD can be eventually transformed into the consistent low-amplitude oscillations for both NN and SW networks. In particular, SWD evolves into the slow spindling oscillations and background tonic oscillations within the NN and SW network, respectively. Our modeling and simulation studies highlight the effect of network topology in the evolutions of SWD and spindling oscillations, which provides new insights into the mechanisms of cortical seizures development.

---

Action Editor: Co-EIC role for Destexhe and Victor

---

✉ Qingyun Wang  
nmqingyun@163.com

Denggui Fan  
worldfandenggui@163.com

Jianzhong Su  
su@uta.edu

Hongguang Xi  
xihongguang@gmail.com

<sup>1</sup> School of Mathematics and Physics, University of Science and Technology Beijing, Beijing 100083, China

<sup>2</sup> Department of Dynamics and Control, Beihang University, Beijing 100191, China

<sup>3</sup> Department of Mathematics, University of Texas at Arlington, Arlington, TX 76019-0408, USA

**Keywords** Spike-wave discharges (SWD) · UP-DOWN state · Spindles · Thalamic reticular nucleus (TRN) · Cortex · Stimulation

## 1 Introduction

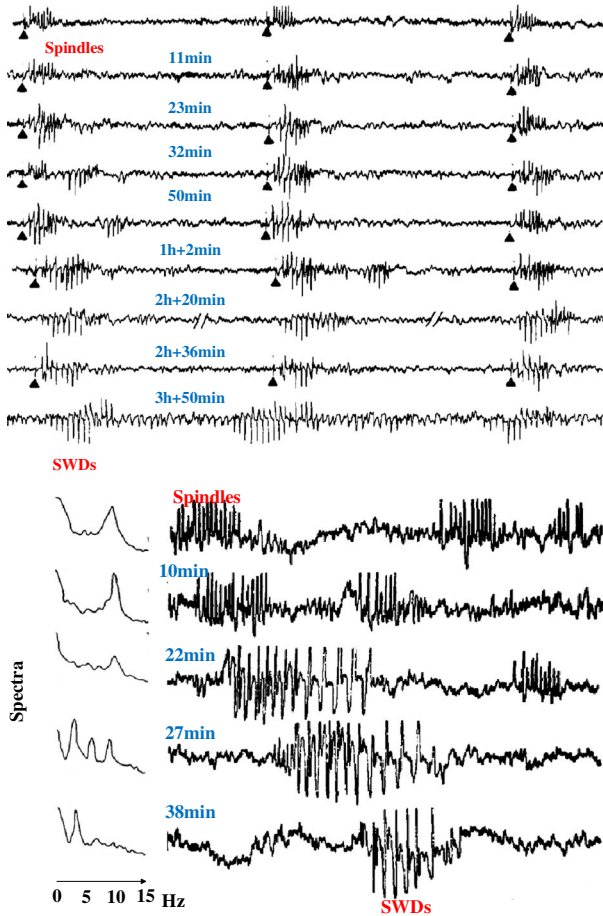
Absence epilepsy, a chronic neurological disorder with petit mal seizures, commonly occurs in the children (Panayiotopoulos 1997). Epileptic absence seizures in humans are characterized by the transient deprivation of consciousness accompanied by well structured bilaterally synchronous periodic ( $\sim 2$ -4Hz) spike-wave discharges (SWD) (Fong et al. 1998). However, rodent models for absence seizures can generate SWD in a relatively fast frequency (5-10 Hz) (Destexhe 1999). Thalamocortical interaction is shown to be critical for the generation of SWD in both the rodent models (Liu et al. 1991) and humans (Moeller et al. 2013). Recurrent  $\sim 2$ -4Hz SWD of absence seizure can also induce the cognitive, linguistic and behavioral disorders (Barnes and Paolichchi 2008; Caplan et al. 2008). Because of chronic nature of these disorders, patients with long term anti-epileptic drug treatment may suffer from drug side-effects (Chen et al. 2017; Loring and Meador 2004). Also, invasive surgery is typically not recommended due to the absence of neuro-radiological abnormalities for absence epilepsy. Potentially alternative therapies to control or suppress the SWD of absence seizure are yet fully explored. Electric stimulus, which can suppress epileptic seizures by aborting the SWD of epileptic brain activities (Taylor et al. 2014; Salem et al. 2016; Blik 2015; Schiller and Bankirer 2007; Su et al. 2008), is considered as a potential supplemental treatment to antiepileptic drugs. However, the dynamic mechanism underlying the spatiotemporal evolutions and abatements of SWD to other firing states, are not well understood.

Spindles are the non-rapid eye movement (NREM) sleep EEG rhythms, i.e., 7-14 Hz in cats (Steriade 2003; Contreras et al. 1997) and 12-15Hz in humans (Rosanova and Ulrich 2005; Steriade 2003), that can occur independently and being correlated to the slow oscillations of 0.6-0.8 Hz (Rosanova and Ulrich 2005) or 0.1-0.2 Hz (Steriade 2003; Steriade et al. 1987). The slow oscillation in human brain is a traveling wave which can periodically sweep the cortex and can form a wave train to trigger the thalamic spindles (Rosanova and Ulrich 2005). Sleep EEG spindling rhythms can also be slow ( $< 13$ Hz) or fast ( $> 13$ Hz) spindles, respectively (Molle et al. 2011; Chatburn et al. 2013). Also, spindles in deep sleep are common brain waves that can be observed in both the normal and abnormal persons. As the normal cortical firing states, spindling activities can be found in the deep sleeping state of the normal persons, but also can be detected in the persons with various typical disorders, such as schizophrenia (Wamsley et al. 2011;

Tsekou et al. 2015; Ferrarelli 2015), Parkinson's disease (Christensen et al. 2014; Latreille 2015) and epilepsy (Boly et al. 2017). In addition, both *in vivo* (Lee et al. 2013; Steriade et al. 1985, 1987) and *in vitro* (Krosigk et al. 1993) recordings suggest that thalamic reticular nucleus (TRN) neurons are spindle pacemakers where the sleep spindles can be abolished after disconnecting SRN (specific relay nucleus) and TRN neurons. Lewis et al. (2015) recently found that TRN can coordinate the slow-wave oscillations of different brain regions to consolidate the new memories and facilitate sharing information. In particular, the spectral power density of NREM sleep EEG slow-wave activity is usually in the range of 0.75–4.5 Hz (Achermann and Borbely 1997; Amzica and Steriade 1997). For example, sleep slow-wave can exhibit characteristic UP-DOWN state with dominant low frequency component ( $< 2$  Hz) (Zhao et al. 2015), through the observations for the local field measurement in the slow-wave sleep state of cortex (Sanchez-Vives and McCormick 2000). Neurophysiologically, the cortical neurons are excessively depolarized in the UP state while the DOWN state involves strong inhibition of cortical neurons.

It has been revealed that the two low-frequency (i.e.,  $< 15$ Hz) conspicuous brain rhythms, SWD and spindle oscillations share the common thalamocortical mechanism (Veggiotti et al. 1999; Tamaki et al. 2008; van Luijtelaaar 1997; Traub et al. 2005). They are induced by the interplays between the GABAergic TRN and the corticopetal SRN, i.e., the thalamic SRN-TRN circuit (Kandel and Buzski 1997; Tamaki et al. 2008; van Luijtelaaar 1997; Kostopoulos et al. 1981; Kostopoulos 2000; Da Silva et al. 2003; Shouse et al. 2000; Steriade et al. 1993). Experimental findings based on a genetic WAG/Rij rat model of absence epilepsy (Meeren et al. 2009; Sitnikova et al. 2010, 2014a, b) also demonstrated that unilateral destructions of both the TRN and its inhibitory projecting target, SRN, can bilaterally abolish the SWD and ipsilaterally abolish the sleep spindles. In particular, absence seizures might inherit some intrinsic properties of sleep spindles, and also sleep spindles can be transformed into the SWD (Kostopoulos et al. 1981; Kostopoulos 2000; Da Silva et al. 2003; Shouse et al. 2000), as shown in Fig. 1a, where the 'spike' component of SWD is originated from the merging of spindle waves (Kostopoulos 2000). However, the connection between non-REM sleep rhythms and SWD is complex and does not seem to point to a simple mechanism. In Fig. 1b we provide ictal recordings of 3 temporal scalp electrodes' EEG from an epileptic patient during sleep, where we can observe the coexistence of spindles and slow-wave oscillations (*Upper panel*), the recurrence of spindles oscillations (*Middle panel*) and the alternative paroxysmal behavior between SWD and spindling activities (*Lower panel*). In addition, the propagation dynamics of SWD and sleep waves are observed in the EEG, MEG and slice models (Golomb et al. 1996; Pinault and

### a Experimental electrophysiology



### b Patient EEG

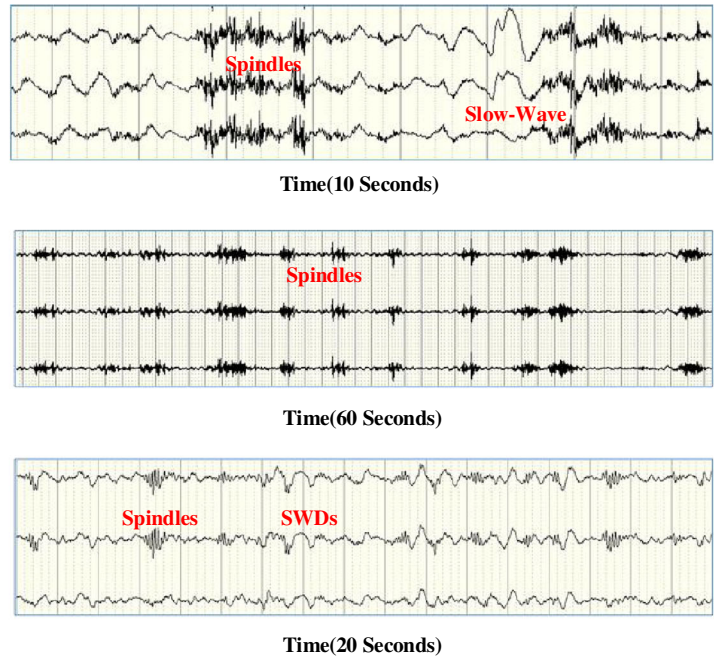


**Fig. 1** (Color online) **a** Experimental electrophysiology modified from Kostopoulos et al. (1981) and Kostopoulos (2000). Upper panel: EEG samples from the middle suprasylvian gyrus of a cat before and after intramuscular injection of penicillin at the times indicated. Triangles indicate the times of single stimuli to nucleus centralis medialis (NCM). Bottom panel: Representative EEG samples from five successive periods of recording before and after the intramuscular injection

of penicillin. **b** Ictal recordings of 3 temporal scalp electrodes' EEG during the epileptic seizures in sleep. Upper panel: 10 s of 3 EEG recordings of an epileptic patient simultaneously show the spindle and slow wave oscillations. Middle panel: 60 s of 3 EEG recordings of an epileptic patient show the reoccurrences of spindling oscillations. Lower panel: 20 s of 3 EEG recordings of an epileptic patient show the alternative occurrences between spindling oscillations and SWD

O'Brien 2005; Shouse et al. 2000; Westmijse et al. 2009; Evangelista et al. 2015).

Computational models provide a potential way to explore the mechanisms underlying the typical 2–4 Hz SWD of epileptic absence seizures and its precursor, spindle oscillations, which have been investigated in numerous previous neural population models (Breakspear et al. 2006; Goodfellow et al. 2011; Taylor et al. 2014; Taylor and Baier 2011; Suffczynski et al. 2004; Sargsyan et al. 2007; Steyn-Ross et al. 2005a, b; Steyn-Ross et al. 2010; Wilson et al. 2005; Yousif and Denham 2005; Drover et al. 2010; Destexhe et al. 1998; O'reilly et al. 2015; Sinha et al. 2014). However, the effect of brain network topology on the emergence of SWD and spindles, as well as the spatiotemporal evolutions between them, have not been well understood. In addition, Taylor et al. (2013, 2014, 2015) developed a thalamocortical

neural field model, as shown in Fig. 2a, to investigate the effects of stimulation on spike-wave discharges (SWD), thereby guiding studies about the initiations and abatements of epileptic absence seizure. Hence, using this single-compartment neural field model (Taylor et al. 2014) we first investigate the transitional dynamics and mechanism between SWD and slow-wave oscillations with the modulation of TRN due to its pacemaker role (Lewis et al. 2015). Next, we will expand the single-compartment thalamocortical neural field model into a coupled thalamocortical model, using 3 thalamocortical compartments with 2 unidirectionally connective configurations, linear and circular structures (Fig. 6a and b), respectively, to explore the spatiotemporal evolutions of the wave states in the different compartments. Finally, in order to demonstrate the qualitative stability of activity evolutions, i.e., independent of the number of nodes

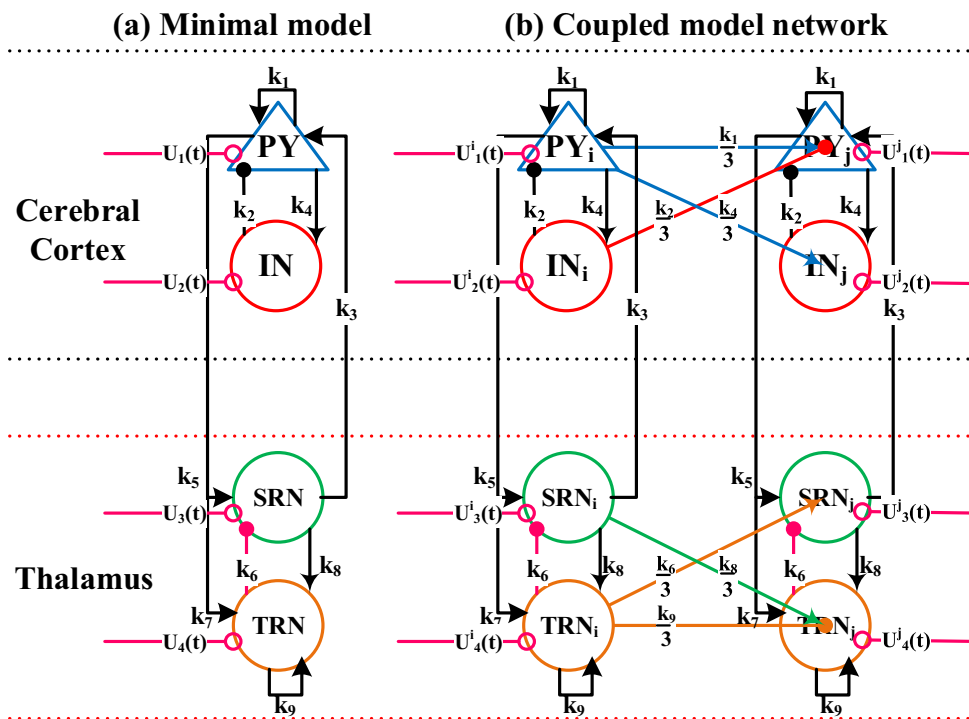


**Fig. 2** (Color online) Schematic diagrams of the computational models. **a** Single-compartment thalamocortical neural field model proposed by Taylor et al. (2014), which is composed of the cortical subnetwork consisting of the excitatory pyramidal neuronal population PY and the inhibitory interneuronal population IN, and the subcortical SRN-TRN circuit model which mainly consists of the specific relay nuclei (SRN) and the thalamic reticular nucleus (TRN) cells (Taylor et al. 2015). **b** A portion of coupled 3 compartments thalamocortical network. The connective mode is the same as the work of Yan

and Li (2011). The lines with arrows indicate the excitatory synaptic functions, and the lines with the closed or open circles represent the inhibitory synaptic functions and the control inputs, respectively. The functions  $k_1, k_2, \dots, k_9$  are the quantitative descriptions of the coupling among the different neuronal populations, PY, IN, SRN and TRN, respectively. The specific parametric values follow the previous works of Taylor et al. (2014, 2015). The function  $k_6$  describes the inhibitory synaptic action from TRN to SRN, which is the critical bifurcation parameter to be considered in this paper

and topological structures of neural network, we further expand the 3-compartment coupled thalamocortical model into the 10-compartment coupled one, with the linear and circular structures (Fig. 6c and d), and the nearest-neighbor (NN) coupled network (Fig. 6e) as well as its realization of small-world (SW) topology via random rewiring (Fig. 6f), respectively. This approach allows to investigate the robustness of SWD spatiotemporal evolutions for network topology.

## 2 Model description and method

### 2.1 Network structure and neural field model

#### 2.1.1 A single-compartment of Taylor model

Neural field model was initially proposed to characterize the macroscopic dynamics of neuronal populations in a low computational cost. Absence seizure are known to arise in the thalamocortical circuit (Evangelista et al. 2015; Liu et al. 1991; Moeller et al. 2013).

Taylor et al. (2014) developed a thalamocortical model (see Fig. 2a for detail), which is based on the thalamocortical loop (Breakspear et al. 2006; Robinson et al. 2002), to investigate the stimulation in spike-wave discharges

(SWD). As shown in Fig. 2(a), the minimal thalamocortical model is composed of the cortical excitatory pyramidal (PY) neuronal population and inhibitory interneuronal (IN) population in cortex area, as well as the subcortical SRN-TRN circuit model consisting of neuron populations of the specific relay nucleus (SRN) and thalamic reticular nucleus (TRN) (Taylor et al. 2014, 2015). The lines with arrows represent the excitatory projections mediated by glutamate. The lines with closed circles denote the  $GABA_A$ -mediated inhibitory projections. Specifically, a single-compartment Taylor model can be described as follows,

$$\frac{dPY}{dt} = (\epsilon_{py} - PY + \kappa_1 F[PY] - \kappa_2 F[IN] + \kappa_3 F[SRN])\tau_1 + u_1(t), \tag{1}$$

$$\frac{dIN}{dt} = (\epsilon_{in} - IN + \kappa_4 F[PY])\tau_2 + u_2(t), \tag{2}$$

$$\frac{dSRN}{dt} = (\epsilon_{sm} - SRN + \kappa_5 F[PY] - \kappa_6 G[TRN])\tau_3 + u_3(t), \tag{3}$$

$$\frac{dTRN}{dt} = (\epsilon_{tm} - TRN + \kappa_7 F[PY] + \kappa_8 G[SRN] - \kappa_9 G[TRN])\tau_4 + u_4(t) \tag{4}$$

where PY represents the excitatory pyramidal neuronal population and IN represents the inhibitory interneuronal population, respectively. The parameters  $\epsilon_{py}$ ,  $\epsilon_{in}$ ,  $\epsilon_{srn}$  and  $\epsilon_{trn}$  are additive constants as used in the original version of Taylor model. The coefficients  $\kappa_1, \kappa_2, \dots, \kappa_9$  are the connectivity strengths within different neuronal populations whose linking rules are in agreement with the experimentally known connection values (Pinault and O’Brien 2005) (also see Fig. 2(a)).  $F(x) = 1/(1 + v^{-x})$  is the sigmoid transition function as used in model of Taylor (2014, 2015), where  $v$  determines the steepness and  $x = PY, IN, SRN, TRN$  in Eqs. (1)–(4).

In particular, in order to simplify the analysis without qualitatively impacting the related dynamics, we simplified the thalamic subsystem by approximating the sigmoid function  $F(x) = 1/(1 + v^{-x})$  with a linear activation term  $G(x) = \alpha x + \beta$ , where  $x = SRN$  and  $TRN$ . This approximation is justified because the thalamic compartment is mainly operating in the linear range of the sigmoid for the SWD. Taylor et al. (2014) shows the qualitative agreement between the two versions of the model with sigmoidal and linear activation functions for the thalamic compartment including the existence of bistable SWD upon perturbation. This also follows the connection schematic as shown in the previous models of Taylor et al. (2014, 2015) and Pinault and O’Brien (2005). In addition, to mimic the effect of stimulation on SWD, we added a stimulus control  $u(t)$ , i.e., a perturbation, on the cortical variables, PY and IN, in the state space.

### 2.1.2 The coupled thalamocortical model network

Spatially-extended networks have also been simulated to study the homogeneous or heterogeneous mode of SWD in cortex (Goodfellow et al. 2011; Taylor and Baier 2011; Fan et al. 2015; Jansen and Rit 1995; Ursino et al. 2010; Sotero et al. 2007). However, these model networks mainly

focused on the macroscopic models of SWD which only incorporate cortico-cortical connectivities. However, sub-cortical structure, especially thalamus, has modulation role in the rhythmic generation mechanisms during absence seizures (Liu et al. 1991; Moeller et al. 2013). Therefore, there is a need for macroscopic models incorporating thalamocortico-thalamocortical connectivities. Further, spike-wave discharges (SWD) and sleep spindles are known to share common thalamo-cortical mechanism (Sitnikova et al. 2014a, b; Tamaki et al. 2008, van Luijtelea et al. 1997). Thus, in this study, we introduce extensions to the original Taylor model by spatially expanding Taylor’s model into multi-compartment coupled network (see Fig. 6). Generally, 2 coupled compartments can be modeled as follows (also see Fig. 2b),

$$\begin{aligned} \frac{dPY_j}{dt} = & (\epsilon_{py} - PY_j + \kappa_1 F[PY_j] - \kappa_2 F[IN_j] \\ & + \kappa_3 F[SRN_j])\tau_1 + u_1^j(t) + \frac{\kappa_1}{m_1} F[PY_i^S] \\ & - \frac{\kappa_2}{m_1} F[IN_i^S] + \frac{\kappa_1}{m_2} F[PY_k^L] + \frac{\kappa_1}{m_3} F[PY_l^D], \end{aligned} \quad (5)$$

$$\begin{aligned} \frac{dIN_j}{dt} = & (\epsilon_{in} - IN_j + \kappa_4 F[PY_j])\tau_2 \\ & + u_2^j(t) + \frac{\kappa_4}{m_1} F[PY_i^S], \end{aligned} \quad (6)$$

$$\begin{aligned} \frac{dSRN_j}{dt} = & (\epsilon_{srn} - SRN_j + \kappa_5 F[PY_j] - \kappa_6 G[TRN_j])\tau_3 \\ & + u_3^j(t) + \frac{\kappa_6}{m_1} G[TRN_i^S], \end{aligned} \quad (7)$$

$$\begin{aligned} \frac{dTRN_j}{dt} = & (\epsilon_{trn} - TRN_j + \kappa_7 F[PY_j] + \kappa_8 G[SRN_j] \\ & - \kappa_9 G[TRN_j])\tau_4 + u_4^j(t) + \frac{\kappa_8}{m_1} G[SRN_i^S] \\ & - \frac{\kappa_9}{m_1} G[TRN_i^S] \end{aligned} \quad (8)$$

**Table 1** Model parameters for the neuronal populations, PY, IN, SRN and TRN

Parametric types	Neuronal populations			
	PY	IN	SRN	TRN
Input Constants	$\epsilon_{py}$ −0.35	$\epsilon_{in}$ −3.4	$\epsilon_{srn}$ −2.0	$\epsilon_{trn}$ −5
Time Scales	$\tau_1$ 26	$\tau_2$ $26 \times 1.25$	$\tau_3$ $26 \times 0.1$	$\tau_4$ $26 \times 0.1$
Control input	$u_1(t)$ −0.3/−0.01	$u_2(t)$ −0.3/−0.01	$u_3(t)$ 0	$u_4(t)$ 0
Transitional Function	$v/\alpha/\beta$ 2.5E5/2.8/0.5	$v/\alpha/\beta$ −	$v/\alpha/\beta$ −	$v/\alpha/\beta$ −

1 PY: Excitatory pyramidal neurons; IN: Inhibitory interneurons; SRN: Thalamocortical relay cells; TRN: Thalamic reticular nucleus

2 “-” represents the values same as PY

where the subscripts  $i, j, k, l \in \{1, 2, \dots, 10\}$  and  $i, k, l < j$  representing the unidirectional connectivity from the pre-compartment  $i, k, l$  to the post-compartment  $j$ .

In addition, it is believed that cortical excitatory pyramidal neurons have sufficiently long axons which can produce significant propagation effect on the distant neuronal populations, while other neural populations can only influence their adjacent areas due to the too short axons. Hereby, three types of inter-minicolumn connections are applied (see Fig. 6g), i.e., S: Short-range connective configurations as shown in Fig. 2b, L: Long-range excitatory connections from pyramidal neuronal populations, D: Distant excitatory connection from pyramidal neuronal populations at some distance. The connective strength,  $k_i$ , is divided by  $m_1=3, m_2=6$  and  $m_3=9$  to respectively describe the effect of S-/L-/D-type of inter-minicolumn connectivities.

### 2.2 Model parameters

Most parameters in the model in this paper are from literature (Taylor et al. 2013, 2014, 2015; Baier et al. 2012, 2017; Taylor and Baier 2011; Fan et al. 2015; Wang et al. 2012) (see also the Tables 1 and 2) which were originally estimated from experimental data. However, due to lack of data, in inter-compartment connectivities, the parameters are estimated in numerical studies. In addition, in order to mimic the effect of stimulus-induced SWD, we performed a stimulus control  $u_i(t)$  on the cortical variables, PY and IN, respectively, where  $u_1(t)$  and  $u_2(t)$  take the values in Table 1, and  $(u_3(t), u_4(t)) = (0, 0)$ . The control parameters are the same as those used in Taylor et al. (2014). During the simulations,  $k_6$  is the bifurcation parameter which varies in the physiologically reasonable range, while the other parameter values are kept the same as the Taylor model.

### 2.3 Simulation method and data analysis

The MATLAB (MathWorks, USA) simulating environment is used to perform the numerical calculations. During the numerical simulations for both the single-compartment

model or 3 coupled compartments networks, differential equations are solved by a standard fourth-order Runge-Kutta solver. Typically models are calculated for more than 20 s, we have the fixed temporal step of 1 ms. The simulation data of a stable state after 10 s are used for the steady state. The bifurcation (Zhao and Robinson 2015; Chen et al. 2014, 2015; Fan et al. 2015) and power spectrum analysis (Zhao et al. 2015; Zhao and Robinson 2015; Chen et al. 2014; Fan et al. 2015) are utilized to describe the occurrences, propagations and transformations of various critical dynamical features generated by our simulation and affected by the stimulations. Firstly, to explore the transitions between various dynamical states, the bifurcation and time frequency analysis are performed for the critical thalamic parameters,  $k_6$ . Therein, the bifurcation diagram is plotted by calculating the stable local minimum and maximum values of the average for the cortical excitatory and inhibitory neuronal populations. To evaluate the dominant frequency of neural oscillations, the spectrograms are estimated using the fast Fourier transform (FFT) for the time series of the average for the cortical excitatory and inhibitory neuronal populations. The maximum peak frequency of power spectral density (PSD) is defined as the dominant frequency. In particular, by combining techniques of both bifurcation and spectrogram analysis, the parametric regions corresponding to typical 2-4 Hz SWD oscillations can be outlined as well as propagations and evolutions of SWD can be observed at these regions.

### 3 Results

Based upon the Taylor model, we first focus on the effects of  $k_6$ , i.e., the coupling strength from TRN to SRN, on the occurrence of the SWD oscillation and its transition dynamics, with the introduction of stimulations or perturbations on the steady state. Next, we use the 3 compartments of thalamocortical field networks to investigate the propagations and evolutions of stimulus-induced epileptic SWD within the different compartments at different  $k_6$  modulation. Finally, we investigate the evolution stability of SWD and spindling

**Table 2** In simulation results depicted in Figs. 3-12, coupling strengths,  $k_1, k_2, \dots, k_9$ , among the four different neuronal populations, PY, IN, TRN and SRN, are as follows

Coupling Strength									
Symbol	$k_1$	$k_2$	$k_3$	$k_4$	$k_5$	$k_6$	$k_7$	$k_8$	$k_9$
Source	PY	IN	SRN	PY	PY	TRN	PY	SRN	TRN
Target	PY	PY	PY	IN	SRN	SRN	TRN	TRN	TRN
values	1.8	1.5	1	4	3	varied <sup>[2]</sup>	3	10.5	0.2

[1] PY: Excitatory pyramidal neurons; IN: Inhibitory interneurons; SRN: Thalamocortical relay cells; TRN: Thalamic reticular nucleus

[2] In Figs. 3a-3b, 3c, 3e/5c-5e, 3f, 4, 3d/5a/7a/8/9a/9c/9d/11/12, 5b and 7b/9b/10, the parameter  $k_6$  is 0-4, 0.1/0.4/1/1.3/3, 1.185, 0-2, 0-5, 0.6, 1.8 and 0.8, respectively

oscillations in complex topology of multimodule neural network with 10 compartments.

### 3.1 Single-compartment neural field model

#### 3.1.1 Thalamic reticular nucleus (TRN)-induced transition from SWD to slow-wave oscillation

In this section, we investigate the transitions of SWD into other firing states induced by the inhibitory synaptic coupling strength of TRN projected into the SRN, as well as the effects of stimulations on the transitions of SWD.

Results in Fig. 3 show that without (Fig. 3a) and with (Fig. 3b) single-pulse stimulations onto the single-compartment system, the model can both display rich dynamics by varying the coupling strength,  $k_6$ , i.e., the inhibitory synaptic function from TRN to SRN, in  $[0, 4]$ . In particular, as shown in the upper panel of Fig. 3a, without stimulation the single-compartment model transits from the high saturated state in ‘I’ (Fig. 3c) to the periodic 1/2-spike and wave discharges in ‘II’ as the parameter  $k_6$  changes in  $[0, 0.49]$ . Successively, transition to the low saturated state (‘III’) occurs when  $k_6$  increases in the region of  $[0.49, 1.17]$ . Afterwards, with  $k_6$  further increasing, the system transits between the bistable low saturated state and SWD in ‘IV’. Finally, for the large value of  $k_6$ , the system transits from low saturated state in ‘V’ into the slow-wave oscillations in ‘VI’, which occurs after around  $k_6 = 1.75$ . In the lower panel of Fig. 3a we present the variation of dominant frequency corresponding to the various firing states within the upper panel of Fig. 3a. From the evolutions of dominant frequencies, we observe several sudden jumps and dives which correspond to the critical transitions of different firing states. Compared the upper panel of Fig. 3a to the low panel of Fig. 3a, we see that the periodic 1/2-spike and wave discharges before left green bar is with at frequency of 2-4Hz, a hallmark of human epileptic absence seizures. While the periodic spike-wave discharge, i.e., SWD, after the right green bar has a relatively faster frequency of 4-10Hz except some single-points. Interestingly, as  $k_6$  further increases, the system can subsequently transit into a low saturated state again. Next, as the value of  $k_6$  passes around  $k_6 = 1.75$ , the system transits into slow-wave oscillations. This is consistent with observed experimental evidences that the increasing synaptic inhibition from TRN to SRN can gradually induce the slow-wave oscillations of deep sleep (Lee et al. 2013; Steriade et al. 1985; Krosigk et al. 1993; Rosanova and Ulrich 2005). Also, with the increasing  $k_6$ , the frequency of simple slow-wave oscillations is gradually increasing in the step-like fashion.

However, after introducing the stimulation, as shown in Fig. 3b, periodic SWD can be induced by the stimulation or perturbation in the parametric region of  $[0.49, 1]$ , indicated

by the two green vertical dashed lines. Physiologically, this means that stimulation may lead to the occurrence of epileptic absence seizures characterized by 2-4Hz SWD, from the background state (i.e., low saturated state). For example, in the Fig. 3d we observe that as  $k_6$  is taken at 0.6, the system initially lies in the background state before  $t = 20$ s. Then, we introduce the single-pulse stimulation at  $t = 20$ s with  $U(t) = (u_1(t), u_2(t), u_3(t), u_4(t)) = (-0.3, -0.3, 0, 0)$ , which represents the small negative perturbations on the system in the background state. After the introduction of stimulation, rhythmic SWD activities can be induced by the single-pulse stimulation indicated by the red vertical bar. Furthermore, the stimulation can also terminate the SWD back into the background low saturated state in the parametric region around  $[1.18, 1.195]$  (see also the red circle in the lower panel of Fig. 3b corresponding to the right black arrow in the upper panel). As shown in the Fig. 3e, when  $k_6$  is taken at a larger value, e.g.,  $k_6 = 1.185$ , the system displays SWD before introducing the stimulation. However, after we add a single-pulse stimulation, i.e.,  $U(t) = (-0.3, -0.3, 0, 0)$  indicated by the red vertical bar, on the system, the SWD is terminated by the stimulation and the system transits from the SWD into the background state.

Compared Fig. 3d to e, it can be inferred that the effect of stimulation on the epileptic SWD can be modulated by the synaptic strength of TRN, i.e.,  $k_6$ . In particular, Fig. 3f shows activity changes with assuming that the inhibitory synaptic coupling strength from TRN to SRN,  $k_6$ , is time-dependent and step-wise increasing for  $0s \leq t \leq 30s$ , as shown in Fig. 3(f<sub>1</sub>). Along with the temporally increasing  $k_6 = k_6(t)$ , without the stimulation, the single-compartment neural field model system displays SWD with the basically decreasing amplitude but the increasing frequencies (Fig. 3(f<sub>2</sub>)). Particularly, as  $k_6$  is increasing into around  $k_6 = 1.6$  with  $t = 22$ s, the amplitudes SWD are damped into the background state. However, as the single-pulse stimulation indicated by the red bar (upper panel of Fig. 3(f<sub>3</sub>)) is introduced at around  $t = 25$ s, the simple slow-wave oscillations (close-up in the upper panel of Fig. 3(f<sub>3</sub>)) with the frequency of  $\sim 5$ Hz (lower panel of Fig. 3(f<sub>3</sub>)) can be induced. Hence, single-pulse stimulations can induce transitions from SWD to slow-wave oscillations.

#### 3.1.2 The dynamical mechanisms underlying the stimulus-induced spike-wave discharges and slow-wave oscillations

In the last section, we have observed rich dynamical behaviors induced by TRN in the modified model. However, the dynamical bifurcation mechanisms underlying these activity transitions are still missing. Hence, in this section, we will elaborate the mechanistic explanations for the bifurcation mechanisms of these transitional behaviors. In particular,

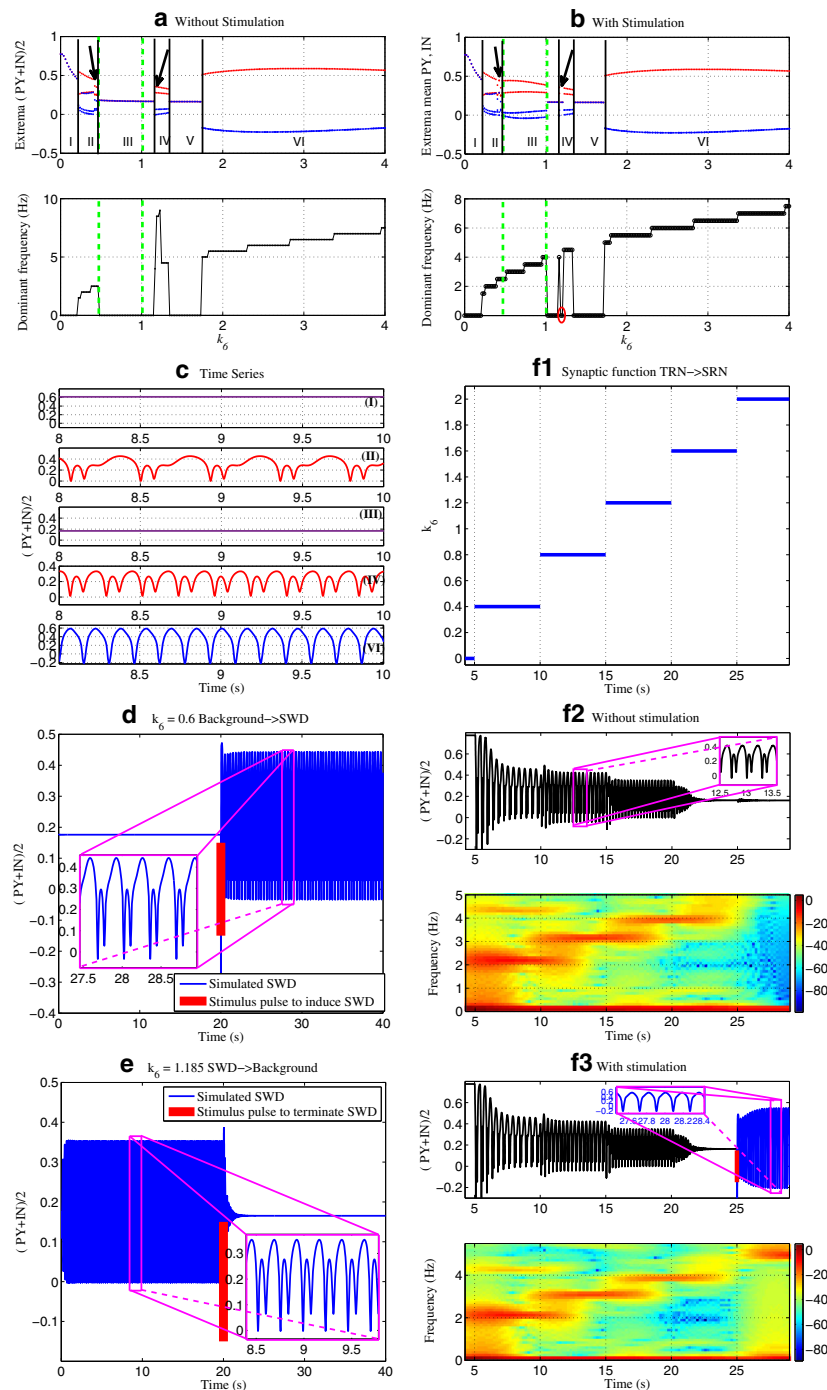


**Fig. 3** (Color online) **a, b** Bifurcation diagrams (upper panels) and corresponding dominant frequencies (lower panels) for a single-compartment model without single-pulse stimulations in **(a)** and with stimulation in **(b)**, as the coupling strength,  $k_6$ , increases in  $[0, 4]$ . **c** The time series corresponding to the different states in **(a)**. The corresponding parameters are set as: (I)  $k_6 = 0.1$  (high saturated state), (II)  $k_6 = 0.4$  (periodic 2-spike and wave discharges), (III)  $k_6 = 1$  (low saturated state), (IV)  $k_6 = 1.3$  (SWD) and (VI)  $k_6 = 3$  (slow-wave oscillations). **d** shows the stimulus-induced periodical SWD at  $k_6 = 0.6$ . The close-ups of **(d)** are 2–4 Hz SWD, i.e., characteristic of epileptic absence seizure. The left black arrow in **(a, b)** indicates the parameter values where the 2-spike and wave discharges can be terminated by a single-pulse stimulation, while within the values of  $k_6$  indicated

by the right black arrow the SWD can be terminated by a single-pulse stimulation, e.g., **e** shows the stimulus-induced terminations of SWD at  $k_6 = 1.185$ . The parametric interval indicated by the two vertical green dashed lines is the interval where stimulations can induce the occurrences of SWD. **(f)** shows the time series as  $k_6$  increasing in a step fashion with time. **(f1)** Synaptic function TRN  $\rightarrow$  SRN, is a step function, increasing for  $t \in [4.3, 29]$  (unit: *sec*). Time series (upper panels) and the corresponding dynamic power spectra (lower panels) are depicted in **(f2)** without stimulations, and the same activities under stimulations are in **(f3)**. Zoom-in panels in **(f2)** and **(f3)** show  $\sim 4$ Hz spike-wave discharges (SWD) and  $\sim 5$ Hz simple slow-wave oscillation, respectively



we will consider Fig. 3a as instance to mechanistically illustrate various dynamical transitions.

In Fig. 4b, the extrema of the model output for different values of  $k_6$  are shown. Compared Fig. 4a to b, we can

see that for the much small values ( $k_6 < \approx 0.2066$ ) there is only one stable fixed point representing the high saturated state of the system. This follows a fold of cycles bifurcation ( $LPC_1$ , Fig. 4b) at  $k_6 \approx 0.2066$  with giving birth to

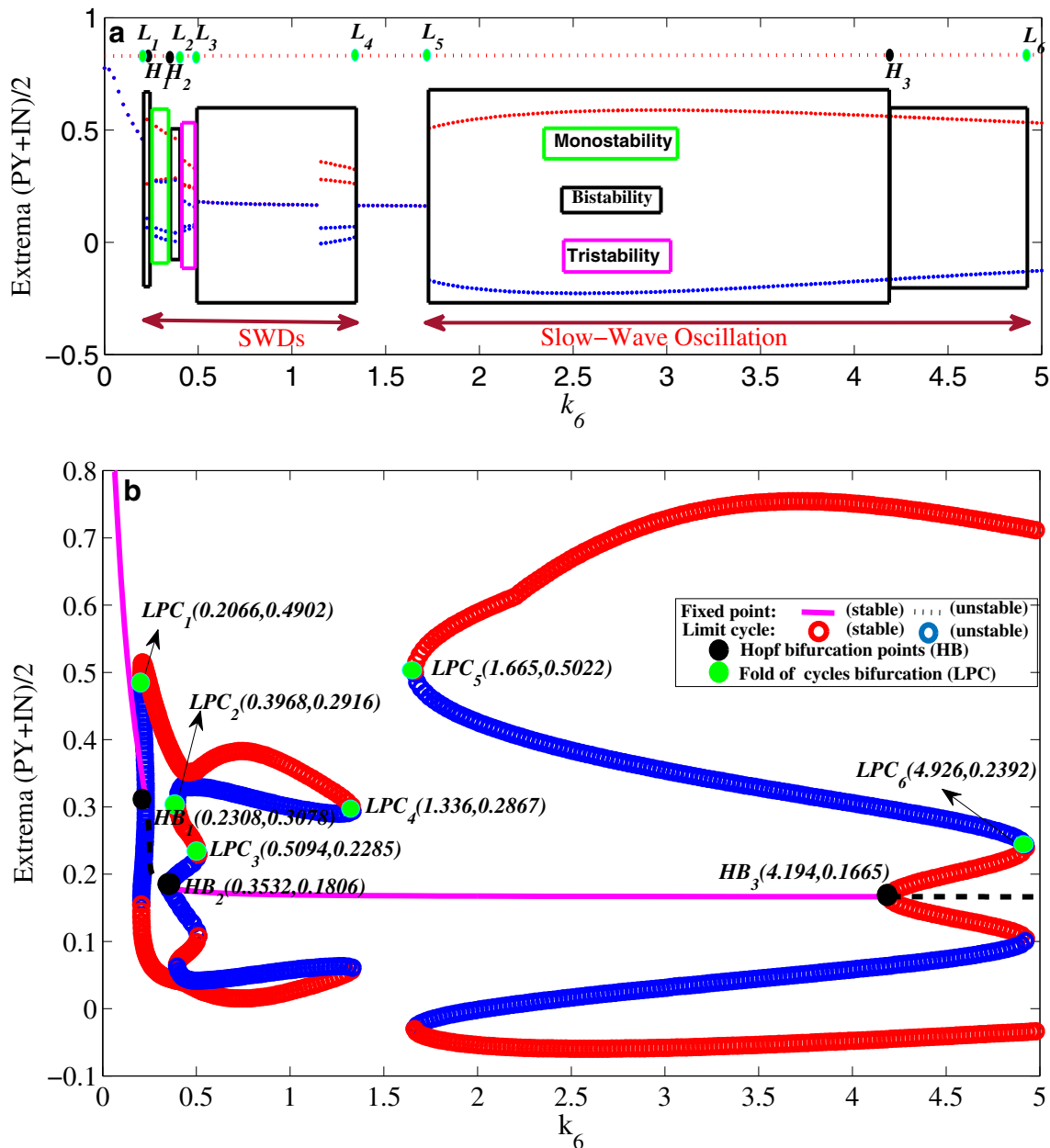


**Fig. 4** **a** Minima and maxima of time series for different values of  $k_6$ , corresponding to Fig. 3a. Colored rectangles represent the multi-stable parameter regions, where green rectangle indicates the monostability, black rectangles represent the bistable regions between non-seizure and SWD states, and pink rectangle corresponds to the tristable region, respectively. The green points indicated by  $L_i$  ( $i = 1, 2, \dots, 6$ ) correspond to the fold of cycles bifurcations (LPC), and the black points indicated by  $H_j$  ( $j = 1, 2, 3$ ) correspond to the Hopf bifurcation points (HB). The horizontal double arrows represent the potential spike wave discharges (SWD) of absence seizures and slow-wave oscillations of clonic epileptic seizures. Therein, the region indicated by the

green rectangle represents the spontaneous SWDs. **b** Dynamical bifurcation diagram corresponding to the various state transitions in (a). As  $k_6$  increasing, the system undergoes six LPC bifurcations indicated by green points and three Hopf bifurcations (HB) indicated by black points, respectively. LPC bifurcations occur at the transition between bistability and excitability. The stabilities of fixed points can be switched around HB bifurcations. Overall, the parameter regions consist of stable fixed point, stable limit cycles, bistable regions composed of stable limit cycle and stable fixed point (or two stable limit cycles with different amplitudes) and tristable region composed of stable fixed point and two stable limit cycles, respectively

one stable limit cycle and one unstable, which results in a bistable region,  $0.2066 < \approx k_6 < \approx 0.2308$ . That is the area of Fig. 4a indicated by the left first black rectangle, with the coexistence of a stable fixed point and a stable limit cycle. Accordingly, the system transits from the high saturated firings to the bistable states between the non-seizure state and SWD oscillations. Then the system enter into a monostable region (i.e.,  $0.2308 < \approx k_6 < \approx 0.3532$ , indicated by the green rectangle) following a subcritical Hopf bifurcation ( $HB_1$ , Fig. 4b), where the stability of fixed points switches. However, the system can restore into the bistable state due to another subcritical Hopf bifurcation ( $HB_2$ , Fig. 4b) at  $k_6 \approx 0.3532$ , which accompanies the switch of fixed points from instability to stability. Particularly, when  $k_6 \approx > 0.3968$ , a tristable region (i.e.,  $0.3968 < \approx k_6 < \approx 0.5094$ , indicated by pink rectangle) with two stable limit cycles and one stable focus arises following the second LPC bifurcation ( $LPC_2$ ) at  $k_6 \approx 0.3968$ . Consecutively, the system can enter into the bistable region again due to the third LPC bifurcation ( $LPC_3$ ) at  $k_6 \approx 0.5094$ . Further, when  $k_6 \approx > 1.336$  but lower than  $k_6 \approx 1.665$ , the bistable region disappears following the fourth LPC bifurcation ( $LPC_4$ ) at  $k_6 \approx 1.336$ . The system transits into the background low saturated state. However, as  $k_6 \approx > 1.665$ , a bistable region reappears due to the fifth LPC bifurcation ( $LPC_5$ ). Compared Fig. 4b to a, we can see that the system then transits from the background low saturated state to simple slow waves (clonic) oscillations. Beyond the reappearance of unstable focus due to the supercritical Hopf bifurcation ( $HB_3$ , Fig. 4b), another bistable region indicated by the last black rectangle (Fig. 4a) and composed of two stable limit cycles with different oscillation amplitudes (Fig. 4b) occurs. In addition, for much large values of  $k_6$  (e.g.,  $k_6 \approx > 4.926$ ), the limit cycles with smaller oscillation amplitude disappears due to another LPC bifurcation ( $LPC_6$ ). Then the system transits into the monostable states again.

Overall, as  $k_6$  increasing, the system can successively transits from high saturated state, SWD and low saturated state to the slow-wave oscillations. However, for the typical values of  $k_6$  within the multistable regions, the system status will be eventually dependent on both the initial values of the four state variables and the applied stimulation perturbations. From the mathematical standpoint, in the bistable region of the four dimensional state space there exists a separating manifold, i.e., separatrix, similar to the blue lines shown in Fig. 4b, even though this manifold of system is structurally complex. In particular, when the initial values for the four state variables are close to the side of separatrix near the stable focus, the system will converge to the steady states, while the system will show the SWD or simple slow-wave oscillations when the initial values are close to the side of separatrix near the stable limit cycle. In addition, stimulation perturbations can change the time

phase of system, which may drive the system beyond the separatrix and hence finally change the states of system. Thereby, as shown in Figs. 3a and b, the system presents rich dynamical transition behaviors, where all the initial values of the four state variables during the simulations are set to  $[0.1724, 0.1803, -0.0818, 0.2775]$ . By contrast, the monostable regions correspond to the spontaneous firing states of the system including the spontaneous SWD (see the region indicated by the green rectangle in Fig. 4a) and slow-wave oscillations.

### 3.1.3 The choice of stimulation parameter

As mentioned above, different activity states can transit between each other by typical single-pulse stimulations that drive the system from one basin of attraction to another. The pulse input, for example, can move a trajectory beyond a separatrix of a saddle point, into the basin of attraction of a steady state. Here, the basin of attraction of background state serves as the target for seizure abating stimuli. In general, a basic of attraction is non spatial-temporally uniform, even for background state. Efficient seizure abating stimuli typically depend on the amplitude and phase of the SWD cycle at the moment of stimulation, as well as the direction of the stimulus in state space. However, it has been demonstrated by the work of Taylor et al. (2014) that fixing the stimulation direction does not restrict the generality of the investigation, we thereby fix the stimulation direction to point to the PY and IN variables in state space and allow stimulation timing and amplitude to vary.

Figure 5a and b show the numerically reconstructed basin of the background state. In Fig. 5a, the basin appears to be closer the SWD attractor, hence SWD can be easily initiated and terminated by typical stimulation perturbations. By contrast, in Fig. 5b, slow-wave attractor appears to surround the basin, thus typical stimulation can induce the slow-wave oscillation from background state. However, the slow wave is not easily terminated into the background state. Figure 5c shows a time series for SWD at  $k_6=1.185$ , where a stimulus of fixed amplitude with  $U(t) = (-0.3, -0.3, 0, 0)$  was applied at different phases/time points. Stimulation outcome are labeled as successful and unsuccessful, colored in pink and cyan when the system can go and not go to background activity, respectively. Here, we observe that during the ascending phase of slow wave component in SWD, the stimulus to the cortical populations can terminate SWD. During the descending phase of slow wave component and the almost whole spike component in SWD, this particular single pulse stimulus can not stop the seizures. Figure 5d is a time series for one deterministic SWD cycle from Fig. 5c. In Fig. 5e, we simultaneously scanning the stimulation time points and stimulation amplitude during the same SWD cycle as Fig. 5d. The scan result is plotted depending

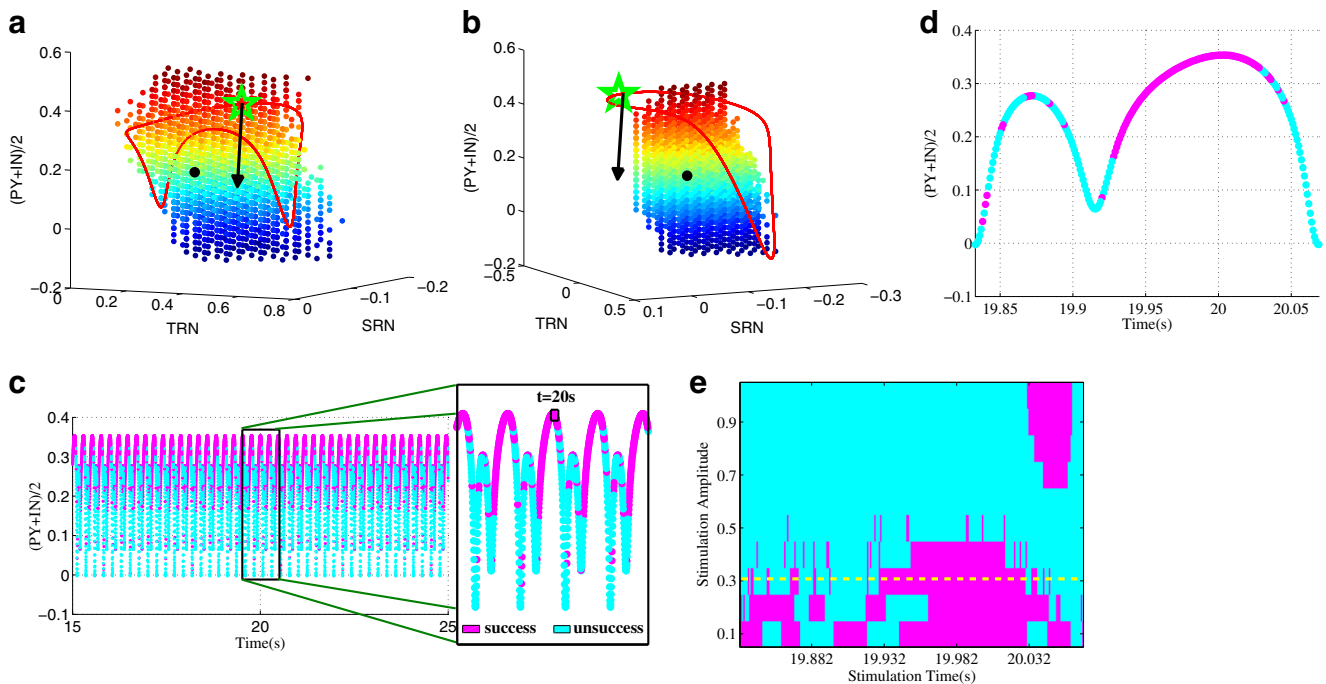


**Fig. 5** (color online) Basin of attraction of the background state in the three dimensional state space corresponding to  $k_6 = 0.6$  (a) and  $k_6 = 1.8$  (b), respectively. Red lines indicate the SWD (a) and slow wave (b) attractors. Black dots indicate the background state. Colored dots are located in the basin of attraction of the background state. The SWD basin of attraction is not specifically shown, as it is simply the part in state space that is not the background basin. Stars show the stimulation timings,  $t=20s$  and  $25s$ , respectively. c SWD firing series at  $k_6 = 1.185$ , where pink sections indicate the stimulation timings when

SWD can be successfully terminated by single-pulse stimulations, while stimulation applied in the cyan sections can not successfully terminate the SWD. d Color coded time series of one cycle of SWD. The pink color indicates a return to the background fixed point if stimulated at the color-coded position using a fixed stimulus amplitude  $U(t) = (-0.3, -0.3, 0, 0)$ . e Color coded map of stimulation amplitude and timing in the same SWD cycle corresponding to (d). The particular amplitude used for (d) has been outlined in a yellow line

on the two scanned parameters. The same color code as in (c) has been used. Yellow dashed line in (e) indicates the stimulation amplitude used in Fig. 5c. We can observe from Fig. 5e that for the majority of the time series, only weaker stimulations stop SWD seizures. This underlines that stronger stimulation does not necessarily lead to better success. There exists a phase in the later part of slow wave component in SWD where only moderate stimulations can not stop SWD oscillations. However, for the ending phase in slow wave component of SWD, termination can always not be achieved by the single-pulse stimulation. However, it is, in essence, the geometry of the basin of attraction that determines the outcome of a stimulation. The success depends on if the stimulus pushed the trajectory to reach over the basin of attraction.

### 3.2 Stimulus-induced propagations and evolutions of SWD to the sleep-like UP-DOWN and spindle oscillations

In the last section, we mainly investigate the transitions of SWD into the slow-wave oscillations at different levels of

$k_6$ , i.e., the synaptic coupling strength from TRN to SRN, and induced by the inhibitory weak single-pulse stimulation or small perturbations. Electrophysiological experiments have long demonstrated transitions between SWD and deep sleep-like slow-wave oscillations including the UP-DOWN and spindle activities (Kostopoulos et al. 1981; Sanchez-Vives and McCormick 2000; Crunelli et al. 2015; Eschenko et al. 2012). In this section, we explore the propagations, evolutions and transformations of SWD into the sleep-like UP-DOWN and spindle states in our network model. Specifically, we consider the 3 compartments of thalamocortical neural field model networks with the open (Fig. 6a) and closed (Fig. 6b) connective configurations. We focus on if these spatially-extended networks provide new dynamical routes to the spontaneous transitions and abatements of epileptic seizure activities.

Connections in 3 coupled compartments are parameterized by connection strengths shown in Table 2. Using this extended network, we have chosen several data points from the connective and stimulating parameter spaces to produce previous experimental findings with the propagations and transitions from the epileptic SWD to the UP-DOWN

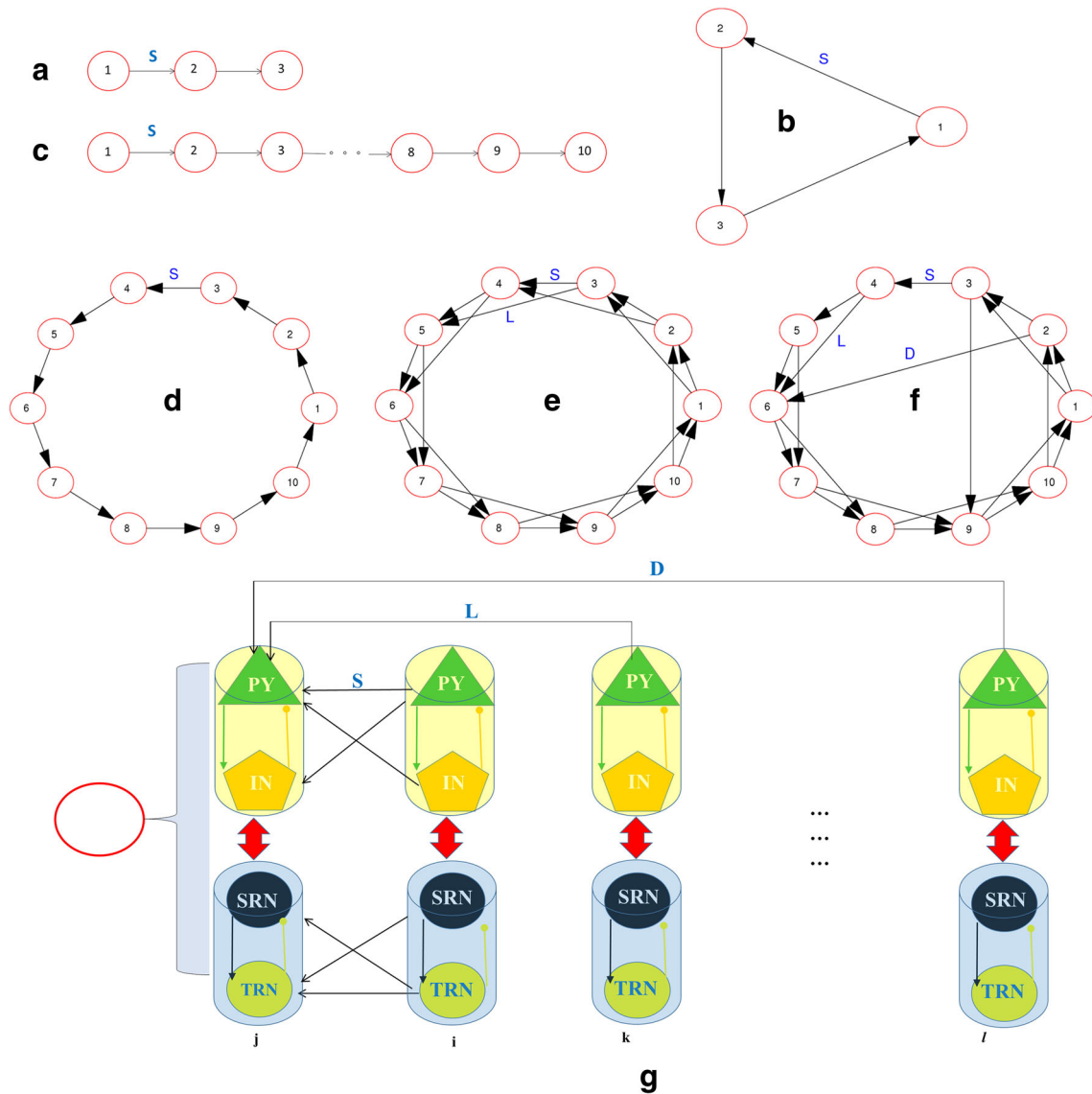


**Fig. 6** (Color online) The unidirectional connective configurations of model network. **a,c** open-ended (or linear) connections; **b,d** closed-ended (circular) connections; **e** Nearest neighbor coupled network characterized by  $p = 0$ . Each vertex is connected to its  $k=2$  nearest neighbors; **f** Realization of small-world topology via random rewiring

of a certain fraction  $p$  of links (in this case 2 out of all 20 were rewired, hence  $p = 0.1$ ); **g** Three connective types of the model network, i.e., S: Short-range connections (see also Fig. 2b), L: Long-range excitatory connection, and D: Distant excitatory connection

and spindles states. The time series for different compartments are generated from stimulation perturbations to the background state of the first compartment. The power spectra derived from the time series and calculated by the fast Fourier transform (FFT) are also used to illustrate the oscillating frequencies.

### 3.2.1 Linearly-extended model network

We first consider the case of open connective model network, as shown in Fig. 6a. In Fig. 7a, we show the time series for the 3 coupled compartments with  $k_6 = 0.6$  ( $a_1$ ) and introducing the stimulation perturbations of  $U^1(t) =$

$(-0.3, -0.3, 0, 0)$ , indicated by the red vertical bar in Fig. 7( $a_1$ ) and ( $b_1$ ), onto the first compartment. Similarly, to Taylor model, without the stimulation (see Fig. 3a), each single-compartment displays the low saturated state as  $k_6 = 0.6$ . Whereas, a single-pulse stimulation can induce SWD as shown in Fig. 3b. In Fig. 7( $a_1$ ), the stimulation is performed onto the first compartment in the background state at  $t = 20s$ . We provide a close-up showing the resulted  $\sim 3Hz$  SWD in epileptic absence seizures. In addition, Figs. 7( $a_2$ ) and ( $a_3$ ) show the time series for the second and third compartments, respectively, displaying the background low-amplitude and high-frequency oscillations. However, compared the Fig. 7( $a_1$ ) with Fig. 7( $a_2$ ) and ( $a_3$ ), due to the

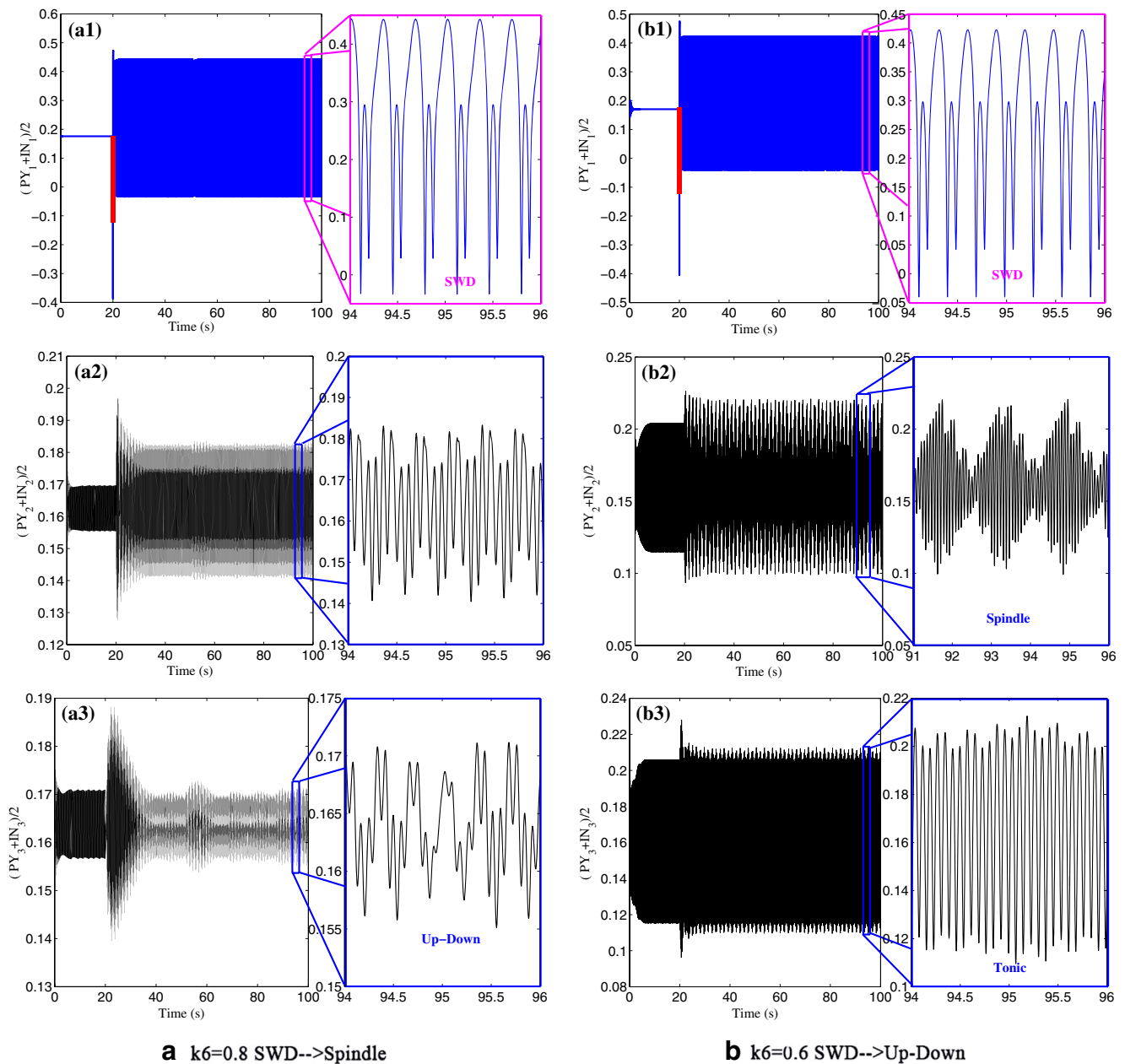


**Fig. 7** (Color online) Simulation results for 3-compartment coupled model network with open connective configuration at  $k_6 = 0.6$  (a) and  $k_6 = 0.8$  (b), respectively. Time series of the average of the excitatory pyramidal neurons and inhibitory interneurons, i.e., (a<sub>1</sub>, b<sub>1</sub>):  $\frac{PY_1+IN_1}{2}$ , (a<sub>2</sub>, b<sub>2</sub>):  $\frac{PY_2+IN_2}{2}$  and (a<sub>3</sub>, b<sub>3</sub>):  $\frac{PY_3+IN_3}{2}$ , respectively. The synaptic stimulation perturbations are  $U^1(t) = (u_1^1(t), u_2^1(t), u_3^1(t), u_4^1(t)) = (-0.3, -0.3, 0, 0)$ ,  $U^2(t) = U^3(t)=0$ , beginning at the red vertical bars. The

zoom-in panels in (a<sub>1</sub>) and (a<sub>3</sub>) show the periodic  $\sim 3$ Hz spike-wave discharges (SWD) and  $\sim 3$ Hz UP-DOWN slow-wave oscillations which are typical in the epileptic absence seizures and deep sleep, respectively. The zoom-in panels in (b<sub>1</sub>), (b<sub>2</sub>) and (b<sub>3</sub>) show the periodic  $\sim 3$ Hz spike-wave discharges (SWD), the spindles, i.e.,  $\sim 13$ Hz waves grouped in sequences that recur with a rhythm of 0.6Hz, and the tonic oscillations with varying amplitude, respectively

successively synaptic propagating effects, different firing states have been induced in the second and third compartments. In particular, when the stimulus-induced SWD in the first compartment propagates into the third compartment, the SWD has transitioned into the slow UP-DOWN state in the deep sleep, as shown in the zoom-in panel of Fig. 7(a<sub>3</sub>).

This may represent the propagations and transitions from epileptic SWD to the sleep UP-DOWN state.

As the inhibitory synaptic function from TRN to SRN, i.e.,  $k_6$ , increases into a larger value at  $k_6 = 0.8$ , each single-compartment also intrinsically remains in the background low saturated states without the stimulation perturbations.

However, under the larger value of  $k_6 = 0.8$ , and a stimulation strength,  $U^1(t) = (-0.3, -0.3, 0, 0)$ , indicated by the red vertical bar and performed onto the first compartment, the system can not only induce the occurrence of  $\sim 3\text{Hz}$  SWD (see Fig. 7(b<sub>1</sub>)), but also induce the generations of deep sleep spindles (see Fig. 7(b<sub>2</sub>)) in the second compartment. The spindle oscillation is characterized by the  $\sim 13\text{Hz}$  waves grouped in sequences with a rhythm of  $\sim 0.6\text{Hz}$ . In addition, the synaptic function from the second compartment can induce the tonic oscillations of the third compartment.

### 3.2.2 Circularly-extended model network

In this section, we consider the closed (or circular) connective model network of the 3 compartments of neural field models. The connective configuration is shown in Fig. 6b.

As shown in Fig. 3a, when  $k_6 = 0.6$  and without stimulation each compartment displays the background resting states. However, as we introduce the relatively weaker stimulation (e.g.,  $U^1(t) = (-0.01, -0.01, 0, 0)$ ) at  $t = 20\text{s}$ , this stimulation can induce the periodic spindles which can also be consistently observed on the whole 3 coupled compartments with the circular coupling, as shown in all Figs. 8(a<sub>1</sub>-a<sub>3</sub>). The spectrograms corresponding to the 3 compartments are given in Fig. 8(a<sub>4</sub>), where the two peaks of  $\sim 0.2\text{Hz}$  and  $\sim 13\text{Hz}$  represent the dominant frequencies between spindle-spindle and oscillations within the single spindle. As shown in the zoom-in panel of Fig. 8(a<sub>1</sub>) the spindles show  $\sim 13\text{Hz}$  oscillations grouped in sequences that repeats with a frequency of  $\sim 0.2\text{Hz}$ . Compare this to the outcome of the clinical situation displayed in the middle panel of Fig. 1b, periodic spindles is qualitatively comparable to the real spindling oscillations, even though in sleep

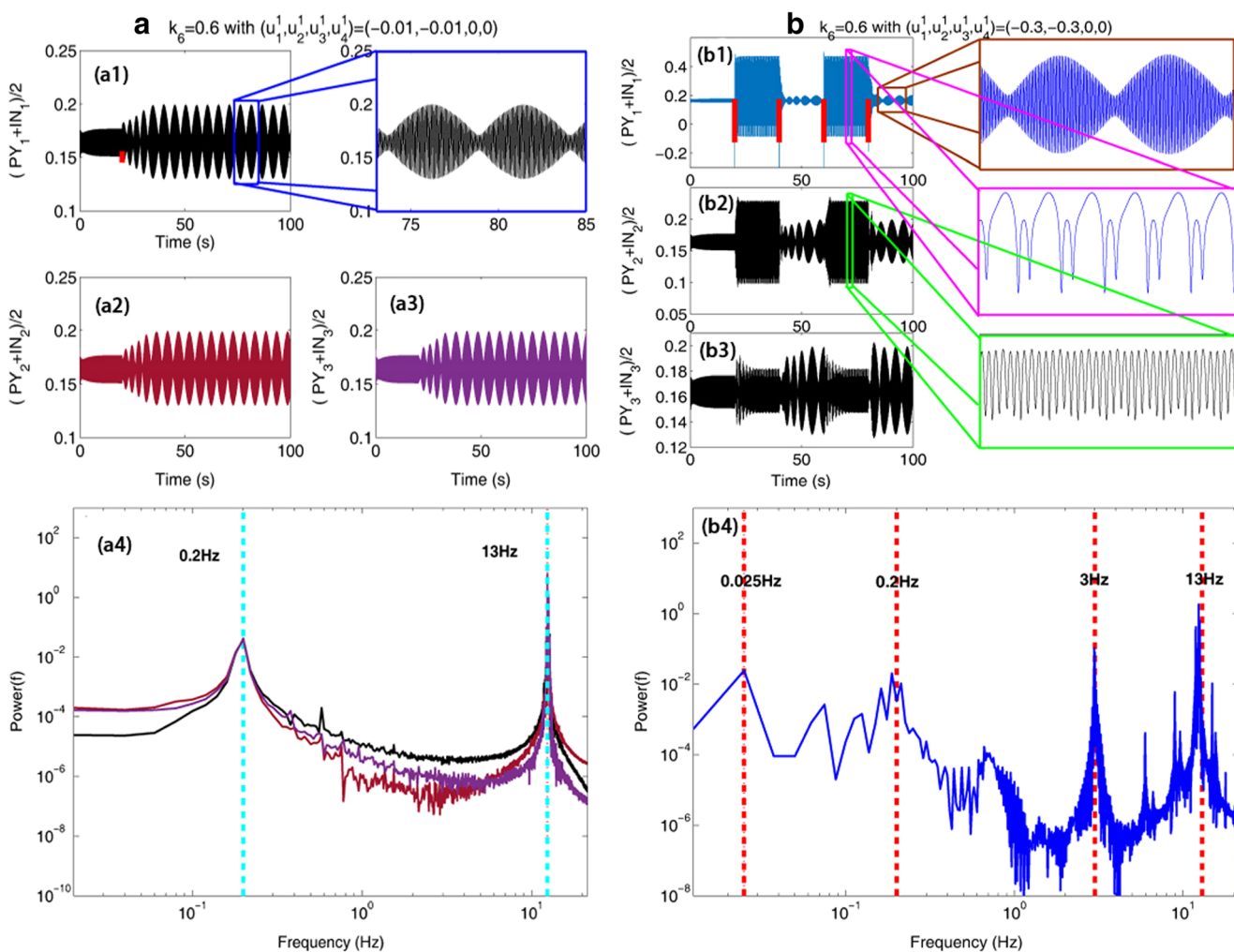


**Fig. 8** (Color online) The simulated results in 3-compartment coupled model network with circularly connective configuration, at  $k_6 = 0.6$  and  $U^1(t) = (u_1^1(t), u_2^1(t), u_3^1(t), u_4^1(t)) = (-0.01, -0.01, 0, 0)$ ,  $U^2(t) = U^3(t) = 0$ . The stimulation is performed at the red vertical bar.

The zoom-in panel in (a) shows the periodic  $\sim 0.2\text{Hz}$  spindles with the rhythmic waves of  $\sim 13\text{Hz}$ . (d): Power spectrums corresponding to the time series show  $13\text{Hz}$  and  $0.2\text{Hz}$  peaks of the spindle waves

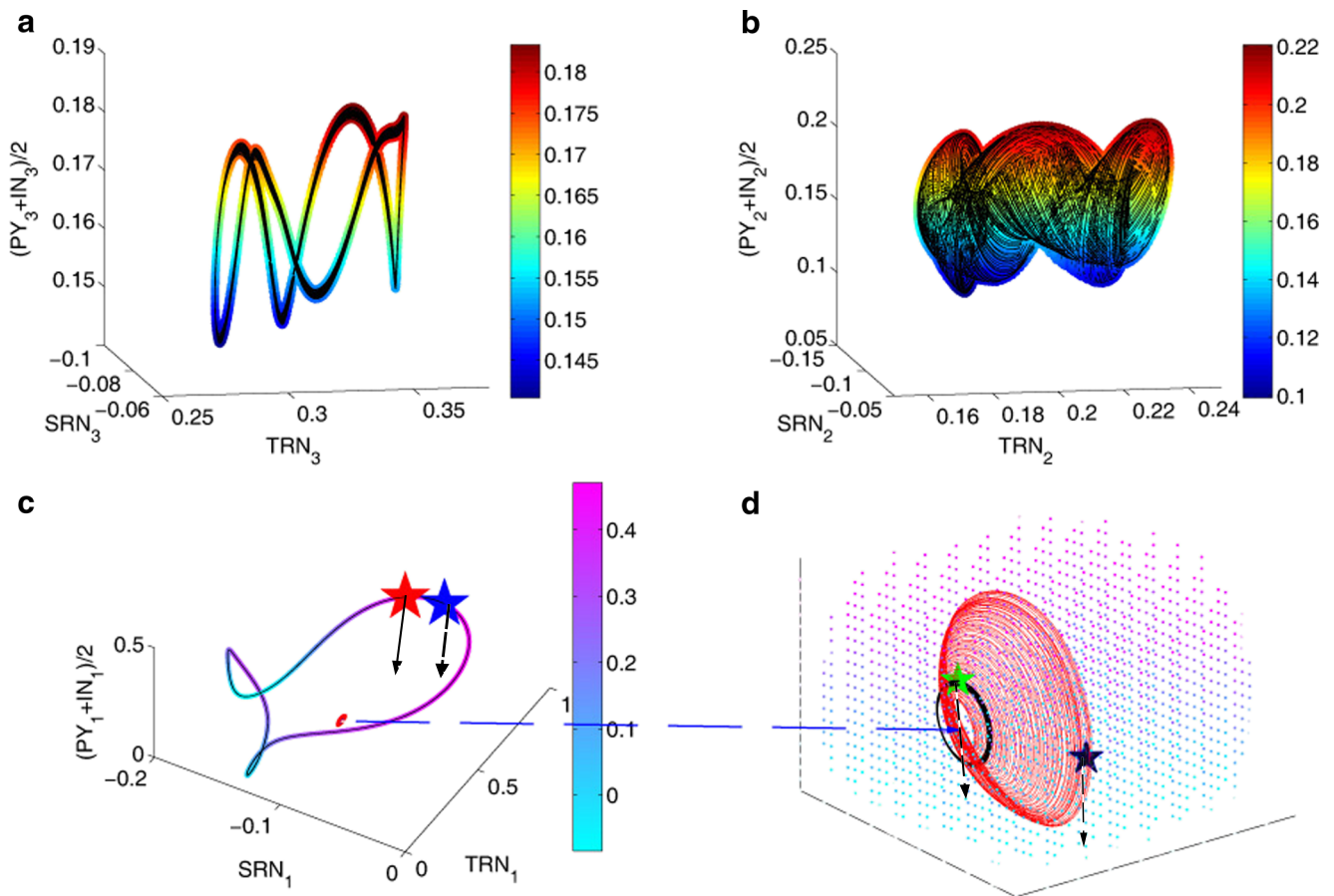


**Fig. 9** (Color online) Phase portrait spanned by the 3 fields  $TRN_{1,2,3}$ ,  $SRN_{1,2,3}$  and  $Mean(PY_{1,2,3}, IN_{1,2,3})$ . **a, b** show the UP-DOWN attractor and spindle attractor, corresponding to the lower panel of Fig. 7a and middle panel of Fig. 7b, respectively. **c** show the SWD attractor, spindle (chaotic) attractors and background tonic (limit cycle) attractor. **d** is the partial close-up of (c), where red shows the

spindle attractor and black shows the tonic attractor. Stars in (c) and (d) represent the stimulation timings in Fig. 8, where green, red, black and blue stars correspond to  $t=20s, 40s, 60s$  and  $80s$ , respectively. Colored dots in (d) show the basin of attraction of the spindle and background states. The part in the state space that is not the spindle and background basin is the SWD basin of attraction

the recurrence of spindles is separated by irregular intervals of arrhythmic dynamic for some seconds.

In order to examine the effect of periodic stimulations on the occurrences and transitions of SWD and spindles, we perform the periodical stimulations indicated by the red vertical bars in Fig. 8(b<sub>1</sub>) onto the first compartment with  $k_6 = 0.6$ ,  $U^1(t) = (-0.3, -0.3, 0, 0)$  and the interstimulus interval  $T = 20s$ . We observe in Fig. 8(b<sub>1</sub>) that periodic single-pulse stimulations initiated at  $t = 20s$  induce the periodic transitions from SWD to spindles illustrated by the zoom-in panels in Fig. 8(b<sub>1</sub>).

The power spectrums corresponding to the time series show the 0.025Hz, 0.2Hz, 3Hz and 13Hz peaks of the mixed mode oscillations in the system, including the SWD and spindles. The frequency of periodic transitions between SWD and spindles is  $\sim 0.025Hz$ , the frequency of SWD is  $\sim 3Hz$ , and the periodic  $\sim 0.2Hz$  spindles is with the rhythmic waves of  $\sim 13Hz$ . In addition, under the circularly connective network, the second and third compartments

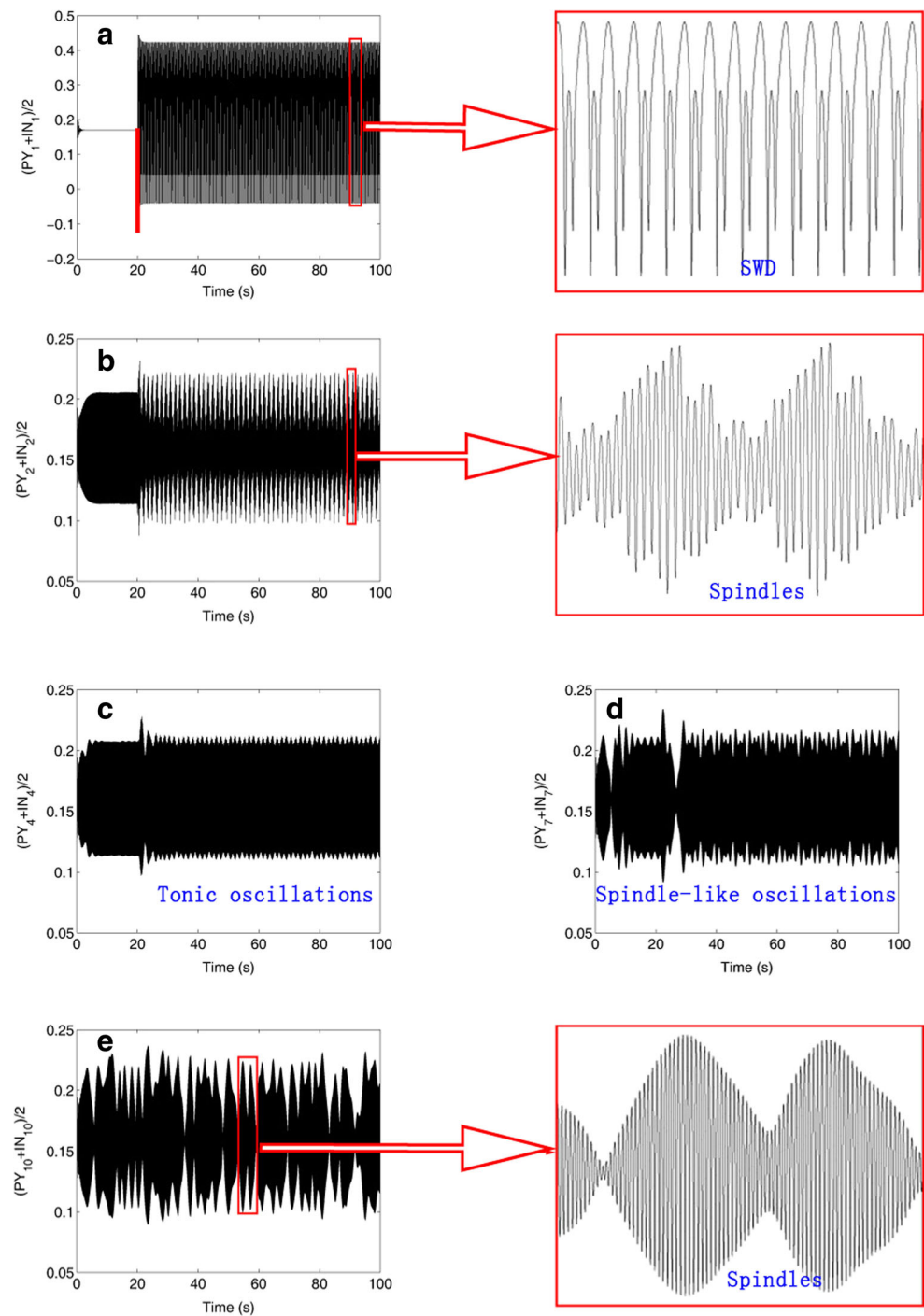
display the periodic transitions between simple tonic oscillations and spindles, hence the effects of periodic stimulations performed on the first compartments can also be found in the second and third ones.

It is noted that Fig. 8(b<sub>3</sub>) shows a transient. This is because when the stimulation effect performed on the first compartment propagates into the third one, it can only induce the transient insufficient initiations. However, we still can observe the evolution effects of multi-rhythmic activities among different compartments. In addition, it can be seen that this alternative mode of transitions between SWD and spindle is qualitatively comparable to the real seizure event shown in the lower panel of Fig. 1b.

### 3.2.3 New dynamics arising from the network model

We begin with coupled network composed of 3 identical thalamocortical subsystems or 3 compartments. As displayed above, the network model can produce the spindling

**Fig. 10** (Color online) The simulation results of 10-compartment model network with linearly connective configuration at  $k_6 = 0.8$  and  $U^1(t) = (u_1^1(t), u_2^1(t), u_3^1(t), u_4^1(t)) = (-0.3, -0.3, 0, 0)$ ,  $U^i(t) = 0$  ( $i=2,3,\dots,10$ ), the single-pulse stimulation at  $t=20s$  is indicated by the red vertical bars in (a)



oscillations in addition to the background state and SWD, even though spindling oscillations were not observed in the single-compartment model. In order to understand the spatiotemporal evolution of these activity states within the various compartments of coupled network, we look into the attractors of the system's behavior and their basins of attraction.

From Figs. 7 and 8, we can infer that the coupled thalamocortical model network dynamics is mainly composed

of seizure attractor, sleeping attractor (UP-DOWN and spindles) and background state attractor. In addition, interactions among the different compartments can be considered as perturbation inputs between each other, which can essentially affect activity states of each subsystem. We use unidirectional connectivity in our model. For each compartment, computational results indicated that the perturbation inputs (coupling strength) received from precompartment is stronger than its perturbation inputs to the postcompartment.



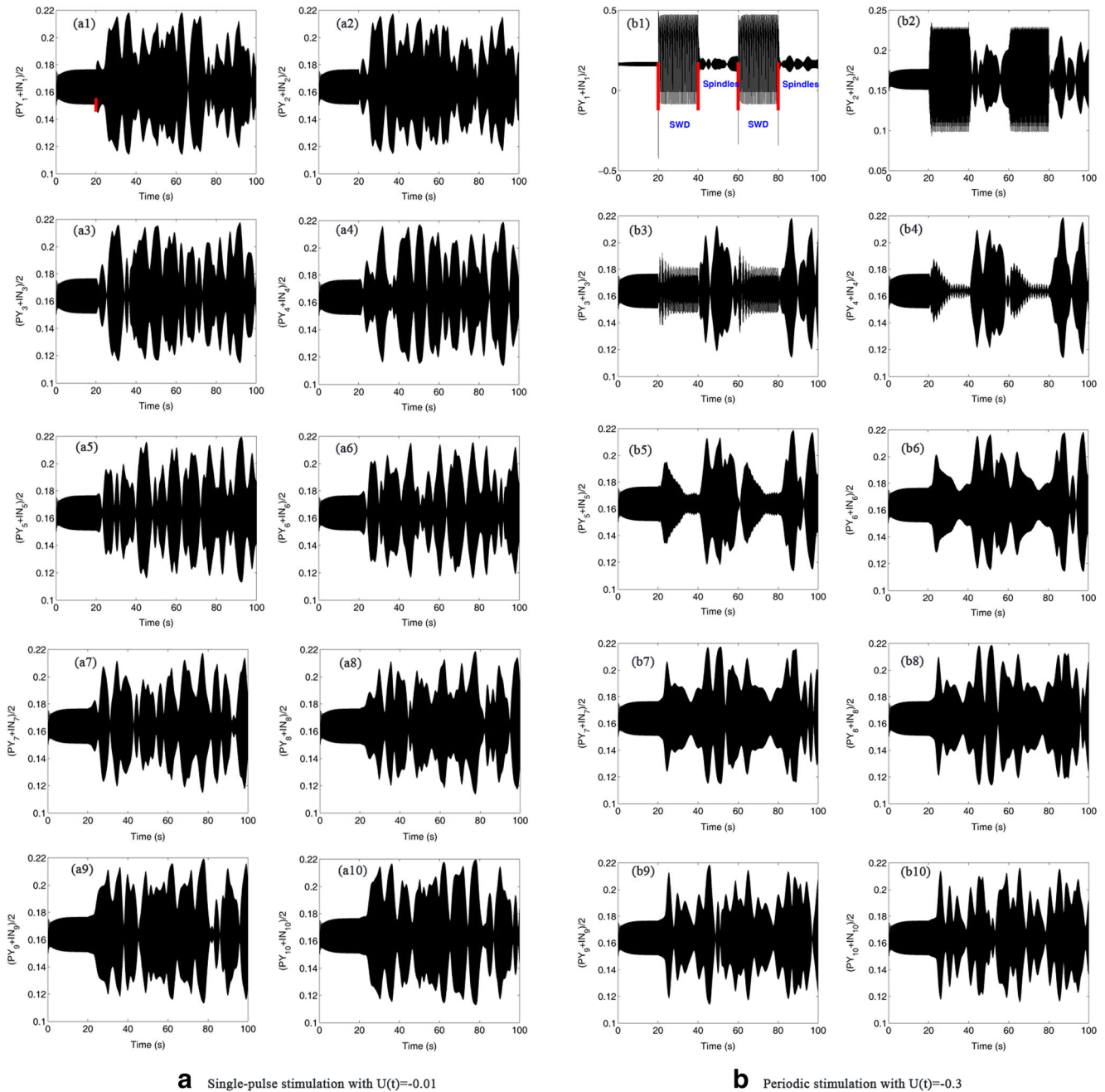


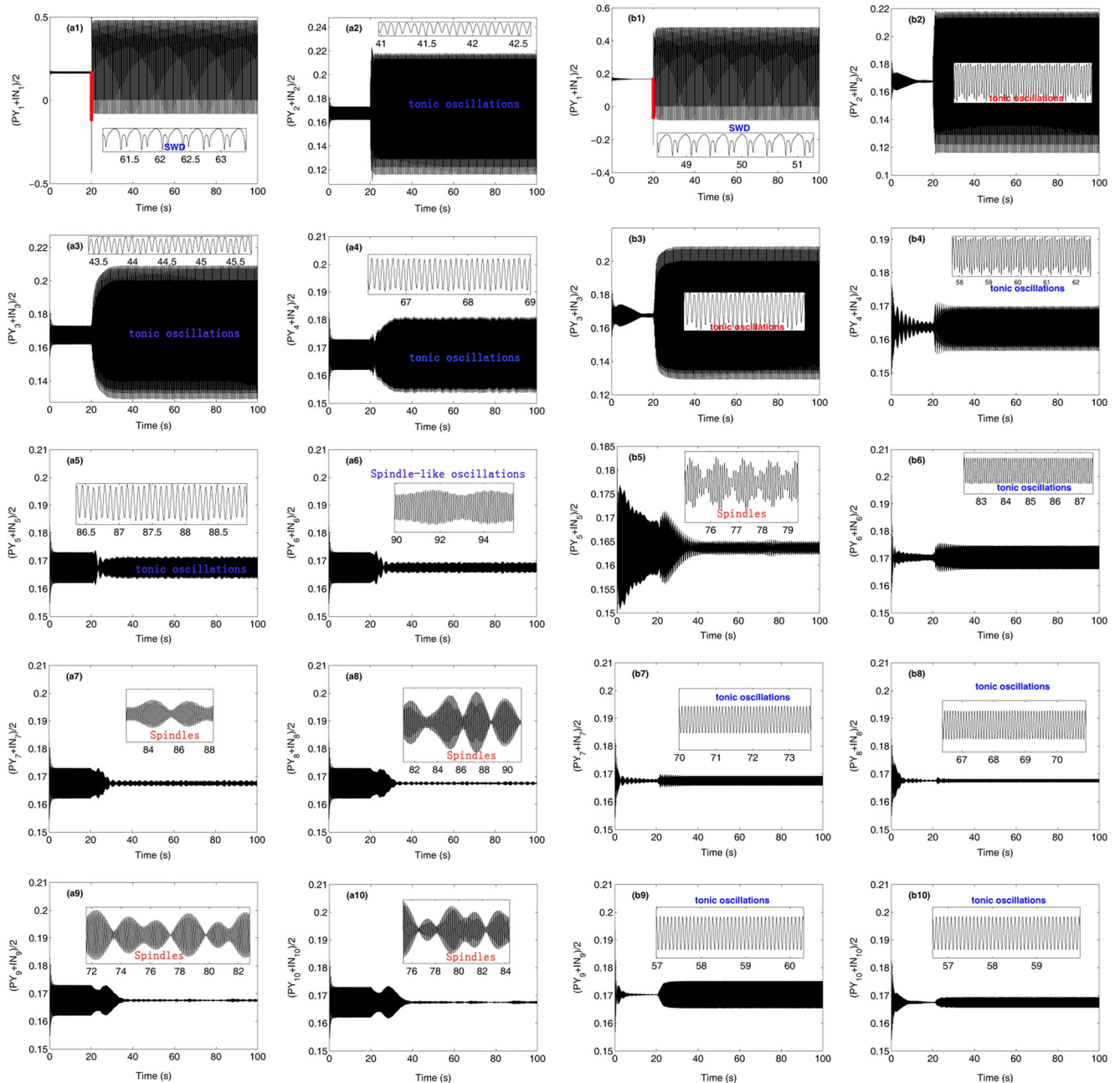
**Fig. 11** (Color online) The simulation results of 10-compartment coupled model network at  $k_6 = 0.6$  with circularly connective configuration. **a** The single-pulse stimulation applied on the first compartment at  $t=20s$  are indicated by the red vertical bars (a1), i.e.,  $U^1(t) =$

$(u_1^1(t), u_2^1(t), u_3^1(t), u_4^1(t)) = (-0.01, -0.01, 0, 0)$ . **b** Periodic stimulations applied on the first compartment are indicated by the red vertical bars in (b1), i.e.,  $U^1(t) = (u_1^1(t), u_2^1(t), u_3^1(t), u_4^1(t)) = (-0.3, -0.3, 0, 0)$ , the period of which is 20s.  $U^i(t)=0$  ( $i=2,3,\dots,10$ )

Network’s strong oscillatory behavior can be spontaneously abated in finite time by impulse inputs.

Figure 9 shows the subsystem slices through the twelve dimensional basin structure of three subsystems by keeping eight model variables constant. Figure 9a and b show the UP-DOWN attractor and spindle attractor corresponding to the Fig. 7(a<sub>3</sub>) and (b<sub>2</sub>), respectively. This is because the

high-amplitude SWD induced by the single-pulse stimulation applied on the first compartment can only make the following compartments reach the basin of the low-amplitude sleeping oscillation or background state attractors, with successively interactive perturbation inputs became weakening along the path. Figure 9c shows the coexistence of three attractors, i.e., SWD attractor, spindle attractor and



**a** Nearest-Neighbor Coupled Network

**b** Small-World Network

**Fig. 12** (Color online) The simulation results of 10-compartment coupled model network at  $k_6 = 0.6$  with two topological connectivities: **a** Nearest-Neighbor Coupled Network:  $U^1(t) = (u_1^1(t), u_2^1(t), u_3^1(t), u_4^1(t)) = (-0.3, -0.3, 0, 0)$ ,  $U^i(t)=0$ , ( $i=2,3,\dots,10$ );

**b** Small-world Network:  $U^1(t) = (-0.25, -0.25, 0, 0)$  and  $U^i(t)=0$ , ( $i=2,3,\dots,10$ ). The single-pulse stimulations applied on the first compartment at  $t=20s$  are indicated by the red vertical bars (a1, b1). The zoom-in panels show the SWD, tonic and spindling oscillations

background state attractor, corresponding to Fig. 8b. Figure 9d is the close-up of Fig. 9(c) showing the basin of attraction of the spindle and background states for the first compartment of circularly coupled network, where the values of the other two subsystems were chosen from the background tonic attractor in order to reduce the impacts of them to first subsystem. It was observed from Fig. 9d that spindle

attractor and background tonic attractor are in close vicinity to each other, such that relatively weaker stimulation perturbation can induce the transitions from background to spindles. Therefore, for the circular network, weak stimulation can induce the spindles within the whole 3-compartment coupled network (see Fig. 8a) by means of the interactive perturbation inputs between different subsystems. Detailed

investigations reveal that only the stimulation strength larger than 0.255 can induce SWD from the background state. Particularly, periodic strong stimulations can drive the system to recurrently shift between the basins of SWD attractor and spindle attractor, hence inducing the periodic transitions between seizure activity and spindling oscillations. Green, red, black and blue stars indicate the typical stimulation positions at  $t=20s$ ,  $40s$ ,  $60s$  and  $80s$ . However, the scenario in first compartment can be weakened when it propagates into the following compartments due to the weak downstream perturbation inputs.

### 3.3 Evolution stability of SWD and spindling oscillations in topology of multimodule neural network

Finally, in order to demonstrate the spatiotemporal evolution robustness of SWD and spindles obtained above, we further expand the 3-compartment coupled thalamocortical model network into the 10-compartment coupled one, with linear and circular structures, and nearest-neighbor (NN) coupled network as well as its realization of small-world (SW) topology via random rewiring, respectively (see Fig. 6).

Figure 10 shows the results of linearly coupled 10-compartment model network. It is seen from Fig. 10 that SWD (Fig. 10a) induced by single-pulse stimulation applied in the first compartment at  $t = 20s$  can first transit into the spindling oscillations of second compartment (Fig. 10b). After that, the system evolves into the simple tonic oscillations (Fig. 10c). However, as the network activities spread into the distant compartments, the system displays the spindle-like oscillations (Fig. 10d), and eventually the consistent irregular spindling oscillations (Fig. 10e). Next, we investigate the evolution effect of SWD within the circularly coupled 10-compartment model network. Similar to the case of 3-compartment model, the first step is to apply weak single-pulse stimulations into the first compartment, i.e.,  $U^1(t) = (-0.01, -0.01, 0, 0)$ , as shown in Fig. 11(a<sub>1</sub>). Consequently, we can see from Fig. 11 that the whole system shows the irregular spindling oscillations, which are qualitatively consistent with those obtained by the 3-compartment models. In particular, when we applied the periodical stronger single-pulse stimulations into the first compartment, as shown in Fig. 11b, we observe the periodical transitions between SWD and irregular spindling oscillations (Fig. 11(b<sub>1</sub>)), which eventually evolve into the consistent irregular spindling oscillations.

To observe the evolutions of SWD within the multi-compartment coupled network with complex topological structures, we consider two topological forms, i.e., nearest-neighbor (NN) coupled network (Fig. 6e) and the realization of small-world (SW) topology via random rewiring of a

certain fraction of links (Fig. 6f). Figure 12 shows the results of NN-/SW-type coupled 10-compartment model network. As a whole, it can be seen from Fig. 12 that with SWD spreading from first compartment to other ones, both the activity wave amplitudes within the two type of coupled networks are gradually decreased. In particular, for the case of NN-type network, SWD firstly transits into the simple tonic oscillations (see Fig. 12(a<sub>2</sub>–a<sub>5</sub>)). As the activity wave propagates into the sixth compartment spindle-like oscillations are induced (Fig. 12(a<sub>6</sub>)), which eventually evolves into the irregular spindling oscillations (Fig. 12(a<sub>7</sub>–a<sub>10</sub>)). In contrast to the NN-type network, SWD eventually evolves into the consistent background tonic oscillations within SW-type network, except for the transient spindling oscillations in the fifth compartment (Fig. 12(b<sub>5</sub>)). This suggests the evolutions of SWD is sensitive to the network topology, given the lower rewiring probability,  $p = 0.01$ , of SW-type network with respect to NN-type network. However, the epileptic SWD can be ultimately transformed into the normal brain activities (spindles and background tonic oscillations), preventing the disease from spreading, which physiologically means the self-regulations of neural system.

## 4 Conclusion and discussion

In this paper, based on the recent experimental findings that thalamic reticular nucleus (TRN) can be the pacemaker of the slow sleep waves (Lee et al. 2013; Lewis et al. 2015; Ferrarelli and Tononi 2017), we began with a minimal single-compartment thalamocortical neural field model to study the effect of TRN on the generations, transitions and propagations of SWD and sleep-like waves including the UP-DOWN and spindle states. It was found that with increasing of the inhibition from TRN to SRN the system can lead to the transitions from SWD to slow-wave oscillation. Particularly, it was shown that stimulation can induce the occurrences of both the SWD and slow-wave oscillation in a specific parametric intervals of TRN, hence leading to the evolutions from SWD to slow-wave oscillations. Then, we considered an extended model networks composed of 3 compartments with the linearly and circularly connective configurations, respectively, to explore propagations among different compartments. It was shown that, for the case of linear connections, stimulation can induce the extended network system to show slow-wave states of brain, especially the UP-DOWN and spindles states. However, for the case of circular connection, weak stimulations can induce the consistent spindle waves, while the stronger periodic single-pulse stimulations can induce the periodic transitions between SWD and spindles. Overall, the cortical closed-ended connectivity benefits the rich waveform transformations in electronic activities, but the cortical open-ended

connectivity facilitates the propagation of activity waves. Furthermore, to demonstrate the evolution robustness of wave activity with respect to the topological structures of neural network, we further expand the 3-compartment coupled network into the larger 10-compartment coupled one, with the linear and circular structures, and the nearest-neighbor (NN) coupled network as well as its realization of small-world (SW) topology via random rewiring, respectively. Interestingly, qualitatively similar results were obtained for the cases of linear and circular connectivities, while NN and SW networks can suppress the brain activity wave into the low-amplitude oscillations.

Slow wave between 0.75 Hz to 4.5 Hz commonly associated with sleeping rhythms of normal human is well known to researchers (Achermann and Borbely 1997; Amzica and Steriade 1997), it can be detected through in-vivo EEG human study. There are also several modeling studies to capture this important feature of sleeping rhythms and explore other transition features (Goodfellow et al. 2011; Taylor et al. 2014; Taylor and Baier 2011, among others). Slow wave is very important for sleeping rhythm study and is a hallmark for classifying sleeping periods (awake, shallow sleep, deep sleep, etc) of a normal human subject. However, our model study focuses on seizure patients, and is on the transition mechanism from SWD to spindle for the specific time period before and after the onset of seizures. In the seizure model, the kind of slow wave 0.75-4.5Hz of normal human cannot be materialized, at least to the extend of this model. In single compartment Taylor model of seizure patient, the slow wave is indeed clonic slow wave, as seen in Fig 3a. The frequency is in the range of 5-10 Hz. Since the type of slow wave observed by (Achermann and Borbely 1997) *in-vivo* EEG of normal person, we have also looked at network model computed results for comparison with normal sleeping rhythm slow wave. We did not observe any typical sleeping slow waves in our network model, but we have observed a mixed mode oscillation of spindles, and the dominant frequency is at 0.2 Hz and a high frequency tonic oscillations of 13Hz (Fig. 8). Thus the seizure patient model reflects a mix of sleeping rhythm and clonic onset. There is a significant difference between normal vs seizure subject.

Neural population models can be used to describe the macroscopic neural activity which can be clinically recorded by EEG. These models provide an effective way to examine the effect of control simulation strategies (Breakspear et al. 2006). In this study, spatially-extended model networks composed of multiple compartments are used to replicate spatiotemporal patterns commonly observed in both the experimental electrophysiology and human EEG during generalized seizures. Exactly, it is compared to traces from different EEG electrodes. In particular, our results that the epileptic SWD can be ultimately transformed into the normal brain activities, i.e., low-amplitude spindles

and background tonic oscillations, can be considered as the self-terminations of epileptic seizures preventing the disease from spreading, which physiologically means the self-regulations of neural system.

However, the connection between non-REM sleep rhythms and epileptic SWD is complex and seems to point to a number of dynamic mechanisms. For example, information transmission delays are inherent to the nervous system (Guo et al. 2016a, b; Wang et al. 2009), which has been widely found to perform key roles in taming neurodynamics, thus inducing transitions between different dynamical patterns. Therefore, more sufficient dynamical mechanisms underlying the transitions between SWD and sleeping UP-DOWN and spindle oscillations still need to be further explored. We hope that our results will inspire testable hypotheses for electrophysiological experiments in the near future.

**Acknowledgements** This research is supported by the National Natural Science Foundation of China (Grant Nos. 11325208, 11572015 and 11172017), the Project funded by China Postdoctoral Science Foundation (Grant No. 2016M600037) and the Fundamental Research Funds for the Central Universities (FRF-TP-16-068A1).

**Author Contributions** DF, QW, JS and HX conceived, designed and performed the research as well as wrote the paper.

#### Compliance with Ethical Standards

**Conflict of interests** The authors declare that they have no conflict of interest.

**Competing financial interests** The authors declare no competing financial interests.

## References

- Achermann, P., & Borbely, A.A. (1997). Low-frequency (<1Hz) oscillations in the human sleep electroencephalogram. *Neuroscience*, 81(1), 213–222.
- Amzica, F., & Steriade, M. (1997). The K-complex: its slow (<1-Hz) rhythmicity and relation to delta waves. *Neurology*, 49(4), 952–959.
- Baier, G., Goodfellow, M., Taylor, P.N., Wang, Y., & Garry, D.J. (2012). The importance of modeling epileptic seizure dynamics as spatio-temporal patterns. *Frontiers in physiology*, 3, 281.
- Baier, G., Taylor, P.N., & Wang, Y. (2017). Understanding epileptiform after-discharges as rhythmic oscillatory transients. *Frontiers in Computational Neuroscience*, 11, 25.
- Barnes, G.N., & Paolicchi, J.M. (2008). Neuropsychiatric comorbidities in childhood absence epilepsy. *Nature Clinical Practice Neurology*, 4(12), 650–651.
- Blik, V. (2015). Electric stimulation of the tuberomammillary nucleus affects epileptic activity and sleep/wake cycle in a genetic absence epilepsy model. *Epilepsy Research*, 109, 119–125.

- Boly, M., Jones, B., Findlay, G., Plumley, E., Mensen, A., Hermann, B., & Maganti, R. (2017). Altered sleep homeostasis correlates with cognitive impairment in patients with focal epilepsy. *Brain: A Journal of Neurology*, *140*(4), 1026–1040.
- Breakspear, M., Roberts, J.A., Terry, J.R., Rodrigues, S., Mahant, N., & Robinson, P.A. (2006). A unifying explanation of primary generalized seizures through nonlinear brain modeling and bifurcation analysis. *Cerebral Cortex*, *16*(9), 1296–1313.
- Caplan, R., Siddarth, P., Stahl, L., Lanphier, E., Vona, P., Gurbani, S., et al. (2008). Childhood absence epilepsy: behavioral, cognitive, and linguistic comorbidities. *Epilepsia*, *49*(11), 1838–1846.
- Chatburn, A., Coussens, S., Lushington, K., Kennedy, D., Baumert, M., & Kohler, M. (2013). Sleep spindle activity and cognitive performance in healthy children. *Sleep*, *36*(2), 237–243.
- Chen, B., Detyniecki, K., Choi, H., Hirsch, L., Katz, A., Legge, A., & Farooque, P. (2017). Psychiatric and behavioral side effects of anti-epileptic drugs in adolescents and children with epilepsy. *European Journal of Paediatric Neurology*, *21*(3), 441–449.
- Chen, M., Guo, D., Li, M., Ma, T., Wu, S., Ma, J., & Yao, D. (2015). Critical roles of the direct GABAergic pallido-cortical pathway in controlling absence seizures. *PLoS Computational Biology*, *11*(10), e1004539.
- Chen, M., Guo, D., Wang, T., Jing, W., Xia, Y., Xu, P., et al. (2014). Bidirectional control of absence seizures by the basal ganglia: a computational evidence. *PLoS Computational Biology*, *10*(3), e1003495.
- Christensen, J.A.E., Nikolic, M., Warby, S.C., Koch, H., Zoetmulder, M., Frandsen, R., et al. (2014). Sleep spindle alterations in patients with parkinson's disease. *Frontiers in Human Neuroscience*, *9*(233), S47–S47.
- Contreras, D., Destexhe, A., & Steriade, M. (1997). Spindle oscillations during cortical spreading depression in naturally sleeping cats. *Neuroscience*, *77*(4), 933–936.
- Crunelli, V., David, F., Lőrincz, M.L., & Hughes, S.W. (2015). The thalamocortical network as a single slow wave-generating unit. *Current Opinion in Neurobiology*, *31*, 72–80.
- Da Silva, F.L., Blanes, W., Kalitzin, S.N., Parra, J., Suffczynski, P., & Velis, D.N. (2003). Epilepsies as dynamical diseases of brain systems: basic models of the transition between normal and epileptic activity. *Epilepsia*, *44*(s12), 72–83.
- Destexhe, A. (1999). Can GABA conductances explain the fast oscillation frequency of absence seizures in rodents?. *European Journal of Neuroscience*, *11*(6), 2175–2181.
- Destexhe, A., Neubig, M., Ulrich, D., & Huguenard, J. (1998). Dendritic low-threshold calcium currents in thalamic relay cells. *Journal of Neuroscience*, *18*(10), 3574–3588.
- Drover, J.D., Schiff, N.D., & Victor, J.D. (2010). Dynamics of coupled thalamocortical modules. *Journal of computational neuroscience*, *28*(3), 605–616.
- Eschenko, O., Magri, C., Panzeri, S., & Sara, S.J. (2012). Noradrenergic neurons of the locus coeruleus are phase locked to cortical up-down states during sleep. *Cerebral Cortex*, *22*(2), 426–435.
- Evangelista, E., Bnar, C., Bonini, F., Carron, R., Colombet, B., Rgis, J., et al. (2015). Does the thalamo-cortical synchrony play a role in seizure termination?. *Frontiers in Neurology*, *6*, 192.
- Fan, D., Wang, Q., & Perc, M. (2015). Disinhibition-induced transitions between absence and tonic-clonic epileptic seizures. *Scientific Reports*, *5*, 12618.
- Ferrarelli, F. (2015). Sleep in patients with schizophrenia. *Current Sleep Medicine Reports*, *1*(2), 150–156.
- Ferrarelli, F., & Tononi, G. (2017). Reduced sleep spindle activity point to a TRN-MD thalamus-PFC circuit dysfunction in schizophrenia. *Schizophrenia Research*, *180*, 36–43.
- Fong, G.C.Y., Shah, P.U., Gee, M.N., Serratosa, J.M., Castroviejo, I.P., Khan, S., et al. (1998). Childhood absence epilepsy with tonic-clonic seizures and electroencephalogram 3C4-Hz spike and multispike slow wave complexes: linkage to chromosome 8q24. *The American Journal of Human Genetics*, *63*(4), 1117–1129.
- Golomb, D., Wang, X.J., & Rinzel, J. (1996). Propagation of spindle waves in a thalamic slice model. *Journal of Neurophysiology*, *75*(2), 750–769.
- Goodfellow, M., Schindler, K., & Baier, G. (2011). Intermittent spike-wave dynamics in a heterogeneous, spatially extended neural mass model. *NeuroImage*, *55*(3), 920–932.
- Guo, D., Chen, M., Perc, M., Wu, S., Xia, C., Zhang, Y., & Yao, D. (2016a). Firing regulation of fast-spiking interneurons by autaptic inhibition. *EPL (Europhysics Letters)*, *114*(3), 30001.
- Guo, D., Wu, S., Chen, M., Perc, M., Zhang, Y., Ma, J., & Yao, D. (2016b). Regulation of irregular neuronal firing by autaptic transmission. *Scientific Reports*, *6*, 26096.
- Jansen, B.H., & Rit, V.G. (1995). Electroencephalogram and visual evoked potential generation in a mathematical model of coupled cortical columns. *Biological Cybernetics*, *73*(4), 357–366.
- Kandel, A., & Buzsáki, G. (1997). Cellular-synaptic generation of sleep spindles, spike-and-wave discharges, and evoked thalamocortical responses in the neocortex of the rat. *Journal of Neuroscience*, *17*(17), 6783–97.
- Kostopoulos, G., Gloor, P., Pellegrini, A., & Gotman, J. (1981). A study of the transition from spindles to spike and wave discharge in feline generalized penicillin epilepsy: microphysiological features. *Experimental Neurology*, *73*(1), 43–54.
- Kostopoulos, G.K. (2000). Spike-and-wave discharges of absence seizures as a transformation of sleep spindles: the continuing development of a hypothesis. *Clinical Neurophysiology*, *111*(s2), S27–38.
- Krosigk, M.V., Bal, T., & McCormick, D.A. (1993). Cellular mechanisms of a synchronized oscillation in the thalamus. *Science*, *261*(5119), 361.
- Latreille, V. (2015). Sleep spindles in parkinson's disease may predict the development of dementia. *Neurobiology of Aging*, *36*(2), 1083–1090.
- Lee, J., Song, K., Lee, K., Hong, J., Lee, H., Chae, S., et al. (2013). Sleep spindles are generated in the absence of t-type calcium channel-mediated low-threshold burst firing of thalamocortical neurons. *Proceedings of the National Academy of Sciences*, *110*(50), 20266.
- Lewis, L.D., Jakob, V., Flores, F.J., Ian, S.L., Wilson, M.A., Halassa, M.M., et al. (2015). Thalamic reticular nucleus induces fast and local modulation of arousal state. *Elife Sciences*, *4*, e08760.
- Liu, Z., Vergnes, M., Depaulis, A., & Marescaux, C. (1991). Evidence for a critical role of GABAergic transmission within the thalamus in the genesis and control of absence seizures in the rat. *Brain Research*, *545*(1), 1–7.
- Loring, D.W., & Meador, K.J. (2004). Cognitive side effects of antiepileptic drugs in children. *Neurology*, *62*(6), 872–877.
- Meeren, H.K., Veening, J.G., Mödersheim, T.A., Coenen, A.M., & van Luijckelaar, G. (2009). Thalamic lesions in a genetic rat model of absence epilepsy: dissociation between spike-wave discharges and sleep spindles. *Experimental Neurology*, *217*(1), 25–37.
- Moeller, F., Muthuraman, M., Stephani, U., Deuschl, G., Raethjen, J., & Siniatchkin, M. (2013). Representation and propagation of epileptic activity in absences and generalized photoparoxysmal responses. *Human Brain Mapping*, *34*(8), 1896–1909.
- Molle, M., Bergmann, T.O., Marshall, L., & Born, J. (2011). Fast and slow spindles during the sleep slow oscillation: Disparate coalescence and engagement in memory processing. *Sleep*, *34*(10), 1411–1421.
- O'reilly, C., Godin, I., Montplaisir, J., & Nielsen, T. (2015). REM Sleep behaviour disorder is associated with lower fast and higher slow sleep spindle densities. *Journal of Sleep Research*, *24*(6), 593–601.

- Panayiotopoulos, C.P. (1997). Absence epilepsies. In Engel, J., & Pedley, T.A. (Eds.) *Epilepsy: A comprehensive textbook* (pp. 2327–2346). Philadelphia: Lippincott-Raven.
- Pinault, D., & O'Brien, T.J. (2005). Cellular and network mechanisms of genetically-determined absence seizures. *Thalamus & Related Systems*, 3(3), 181.
- Robinson, P.A., Rennie, C.J., & Rowe, D.L. (2002). Dynamics of large-scale brain activity in normal arousal states and epileptic seizures. *Physical Review E*, 65(4), 041924.
- Rosanova, M., & Ulrich, D. (2005). Pattern-specific associative long-term potentiation induced by a sleep spindle-related spike train. *Journal of Neuroscience*, 25(41), 9398.
- Salem, K.M., Goodger, L., Bowyer, K., Shafafy, M., & Grevitt, M.P. (2016). Does transcranial stimulation for motor evoked potentials (TcMEP) worsen seizures in epileptic patients following spinal deformity surgery?. *European Spine Journal*, 25(10), 3044–3048.
- Sanchez-Vives, M.V., & McCormick, D.A. (2000). Cellular and network mechanisms of rhythmic recurrent activity in neocortex. *Nature Neuroscience*, 3(10), 1027.
- Sargsyan, A., Sitnikova, E., Melkonyan, A., Mkrtchian, H., & van Luijtelaar, G. (2007). Simulation of sleep spindles and spike and wave discharges using a novel method for the calculation of field potentials in rats. *Journal of Neuroscience Methods*, 164(1), 161–176.
- Schiller, Y., & Bankirer, Y. (2007). Cellular mechanisms underlying antiepileptic effects of low- and high-frequency electrical stimulation in acute epilepsy in neocortical brain slices *in vitro*. *Journal of Neurophysiology*, 97(3), 1887–1902.
- Shouse, M.N., Farber, P.R., & Staba, R.J. (2000). Physiological basis: How nrem sleep components can promote and rem sleep components can suppress seizure discharge propagation. *Clinical Neurophysiology*, 111(S2), S9–S18.
- Sinha, N., Taylor, P.N., Dauwels, J., & Ruths, J. (2014). Development of optimal stimuli in a heterogeneous model of epileptic spike wave oscillations. *IEEE International Conference on Systems, Man and Cybernetics, 2014*, 3160–3165.
- Sitnikova, E. (2010). Thalamo-cortical mechanisms of sleep spindles and spike-wave discharges in rat model of absence epilepsy (a review). *Epilepsy Research*, 89(1), 17–26.
- Sitnikova, E., Hramov, A.E., Grubov, V., & Koronovsky, A.A. (2014a). Age-dependent increase of absence seizures and intrinsic frequency dynamics of sleep spindles in rats. *Neuroscience Journal*, 2014, 370764.
- Sitnikova, E., Hramov, A.E., Grubov, V., & Koronovsky, A.A. (2014b). Time-frequency characteristics and dynamics of sleep spindles in WAG/trj rats with absence epilepsy. *Brain Research*, 1543, 290–299.
- Sotero, R.C., Trujillo-Barreto, N.J., Iturria-Medina, Y., Carbonell, F., & Jimenez, J.C. (2007). Realistically coupled neural mass models can generate EEG rhythms. *Neural Computation*, 19(2), 478–512.
- Steriade, M. (2003). The corticothalamic system in sleep. *Frontiers in Bioscience A Journal & Virtual Library*, 8(1-3), d878.
- Steriade, M., Deschnes, M., Domich, L., & Mulle, C. (1985). Abolition of spindle oscillation in thalamic neurons disconnected from nucleus reticularis thalami. *Journal of Neurophysiology*, 54(6), 1473.
- Steriade, M., Domich, L., Oakson, G., & Deschenes, M. (1987). The deafferented reticular thalamic nucleus generates spindle rhythmicity. *Journal of Neurophysiology*, 57(1), 260–273.
- Steriade, M., McCormick, D.A., & Sejnowski, T.J. (1993). Thalamo-cortical oscillations in the sleeping and aroused brain. *Science*, 262(5134), 679.
- Steyn-Ross, D.A., Steyn-Ross, M.L., Sleigh, J.W., Wilson, M.T., Gillies, I.P., & Wright, J.J. (2005a). The sleep cycle modelled as a cortical phase transition. *Journal of Biological Physics*, 31(3-4), 547–569.
- Steyn-Ross, M.L., Steyn-Ross, D.A., Sleigh, J.W., Wilson, M.T., & Wilcocks, L.C. (2005b). Proposed mechanism for learning and memory erasure in a white-noise-driven sleeping cortex. *Physical Review E*, 72(6), 061910.
- Steyn-Ross, A., & Steyn-Ross, M. (2010). *Modeling phase transitions in the brain*. New York: Springer.
- Su, Y., Radman, T., Vaynshteyn, J., Parra, L.C., & Bikson, M. (2008). Effects of high-frequency stimulation on epileptiform activity *in vitro*: ON/OFF control paradigm. *Epilepsia*, 49(9), 1586–1593.
- Suffczynski, P., Kalitzin, S., & Silva, F.H.L.D. (2004). Dynamics of non-convulsive epileptic phenomena modeled by a bistable neuronal network. *Neuroscience*, 126(2), 467–484.
- Tamaki, M., Matsuoka, T., Nittono, H., & Hori, T. (2008). Fast sleep spindle (13–15 Hz) activity correlates with sleep-dependent improvement in visuomotor performance. *Sleep*, 31(2), 204.
- Taylor, P.N., & Baier, G. (2011). A spatially extended model for macroscopic spike-wave discharges. *Journal of Computational Neuroscience*, 31(3), 679–684.
- Taylor, P.N., Baier, G., Cash, S.S., Dauwels, J., Slotine, J.J., & Wang, Y. (2013). A model of stimulus induced epileptic spike-wave discharges. *IEEE Symposium on Computational Intelligence, Cognitive Algorithms, Mind, and Brain (CCMB)*, 9(5), 53–59.
- Taylor, P.N., Thomas, J., Sinha, N., Dauwels, J., Kaiser, M., Thesen, T., & Ruths, J. (2015). Optimal control based seizure abatement using patient derived connectivity. *Frontiers in Neuroscience*, 1(9), 202.
- Taylor, P.N., Wang, Y., Goodfellow, M., Dauwels, J., Moeller, F., Stephani, U., et al. (2014). A computational study of stimulus driven epileptic seizure abatement. *PLoS one*, 9(12), e114316.
- Traub, R.D., Contreras, D., Cunningham, M.O., Murray, H., Lebeau, F.E.N., Roopun, A., et al. (2005). Single-column thalamocortical network model exhibiting gamma oscillations, sleep spindles, and epileptogenic bursts. *Journal of Neurophysiology*, 93(4), 2194–2232.
- Tsekou, H., Angelopoulos, E., Paparrigopoulos, T., Golemati, S., Soldatos, C.R., Papadimitriou, G.N., et al. (2015). Sleep eeg and spindle characteristics after combination treatment with clozapine in drug-resistant schizophrenia: a pilot study. *Journal of Clinical Neurophysiology*, 32(2), 159–63.
- Ursino, M., Cona, F., & Zavaglia, M. (2010). The generation of rhythms within a cortical region: analysis of a neural mass model. *NeuroImage*, 52(3), 1080–1094.
- van Luijtelaar, E.L. (1997). Spike-wave discharges and sleep spindles in rats. *Acta Neurobiologiae Experimentalis*, 57(2), 113–121.
- Veggiotti, P., Beccaria, F., Guerrini, R., Capovilla, G., & Lanzi, G. (1999). Continuous spike-and-wave activity during slow-wave sleep: syndrome or eeg pattern?. *Epilepsia*, 40(11), 1593–1601.
- Wamsley, E.J., Tucker, M.A., Shinn, A.K., Ono, K.E., McKinley, S.K., Ely, A.V., et al. (2011). Reduced sleep spindles and spindle coherence in schizophrenia: mechanisms of impaired memory consolidation?. *Biological Psychiatry*, 71(2), 154–161.
- Wang, Q., Perc, M., Duan, Z., & Chen, G. (2009). Synchronization transitions on scale-free neuronal networks due to finite information transmission delays. *Physical Review E*, 80(2), 026206.
- Wang, Y., Goodfellow, M., Taylor, P.N., & Baier, G. (2012). Phase space approach for modeling of epileptic dynamics. *Physical Review E*, 85(6), 061918.
- Westmijse, I., Ossenblok, P., Gunning, B., & Van, L.G. (2009). Onset and propagation of spike and slow wave discharges in human absence epilepsy: a meg study. *Epilepsia*, 50(12), 2538–2548.
- Wilson, M.T., Steyn-Ross, M.L., Steyn-Ross, D.A., & Sleigh, J.W. (2005). Predictions and simulations of cortical dynamics during natural sleep using a continuum approach. *Physical Review E*, 72(5), 051910.

- Yan, B., & Li, P. (2011). An integrative view of mechanisms underlying generalized spike-and-wave epileptic seizures and its implication on optimal therapeutic treatments. *PloS one*, 6(7), e22440.
- Yousif, N.A., & Denham, M. (2005). A population-based model of the nonlinear dynamics of the thalamocortical feedback network displays intrinsic oscillations in the spindling (7C14 Hz) range. *European Journal of Neuroscience*, 22(12), 3179–3187.
- Zhao, X., Kim, J.W., & Robinson, P.A. (2015). Slow-wave oscillations in a corticothalamic model of sleep and wake. *Journal of Theoretical Biology*, 370, 93–102.
- Zhao, X., & Robinson, P.A. (2015). Generalized seizures in a neural field model with bursting dynamics. *Journal of Computational Neuroscience*, 39(2), 197–216.